

Review

# A Short Review on Ni Based Catalysts and Related Engineering Issues for Methane Steam Reforming

Eugenio Meloni , Marco Martino  and Vincenzo Palma

Department of Industrial Engineering, University of Salerno, Via Giovanni Paolo II, 132-84084 Fisciano (SA), Italy; mamartino@unisa.it (M.M.); vpalma@unisa.it (V.P.)

\* Correspondence: emeloni@unisa.it; Tel.: +39-089969275

Received: 24 February 2020; Accepted: 20 March 2020; Published: 22 March 2020

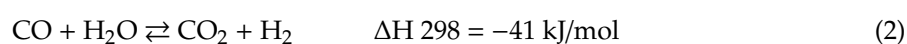


**Abstract:** Hydrogen is an important raw material in chemical industries, and the steam reforming of light hydrocarbons (such as methane) is the most used process for its production. In this process, the use of a catalyst is mandatory and, if compared to precious metal-based catalysts, Ni-based catalysts assure an acceptable high activity and a lower cost. The aim of a distributed hydrogen production, for example, through an on-site type hydrogen station, is only reachable if a novel reforming system is developed, with some unique properties that are not present in the large-scale reforming system. These properties include, among the others, (i) daily startup and shutdown (DSS) operation ability, (ii) rapid response to load fluctuation, (iii) compactness of device, and (iv) excellent thermal exchange. In this sense, the catalyst has an important role. There is vast amount of information in the literature regarding the performance of catalysts in methane steam reforming. In this short review, an overview on the most recent advances in Ni based catalysts for methane steam reforming is given, also regarding the use of innovative structured catalysts.

**Keywords:** methane steam reforming; Ni based catalysts; structured catalysts for methane steam reforming; process intensification

## 1. Introduction

Hydrogen is an important raw material in the chemical industry, and, in the last years, its importance as alternative energy carrier has increased due to the depletion of fossil fuels and increasing environmental concerns. An important consideration about hydrogen is that, since it is an energy carrier and not an energy source, it must be first produced, and then it can be used. Hydrogen can be produced through different processes, such as natural gas or biogas reforming, gasification of coal and biomass, water electrolysis, water splitting by high temperature heat, photoelectrolysis, and biological processes [1]. Some published statistical researches have speculated that a 6% increase or more in hydrogen production will be reached every year [2]. Currently, among the above cited processes, the conventional large-scale production of hydrogen is mainly obtained by two different processes, both fully developed at industrial level: reforming of fossil fuels and water-electrolysis, even if this last process concurs for only 5% of hydrogen produced [1]. The reforming processes include steam reforming, partial oxidation, dry reforming, and auto-thermal reforming [3]. Among the reforming processes, the Methane Steam Reforming (MSR) technology is the oldest and most feasible route to convert CH<sub>4</sub> into H<sub>2</sub>. It is normally described as the result of the reforming (Equation (1)) and the Water Gas Shift (WGS) reactions (Equation (2)),



The produced syngas is in a high H<sub>2</sub>/CO ratio, 3:1. The high endothermicity of the reforming reaction requires operating temperatures that are higher than 700 °C, and Steam-to-methane ratios of 2.5–3.0 are commonly used to reduce coke formation. Accordingly, the MSR process is carried out in industrial furnaces and sustained by burning some portion of the natural gas; as a consequence, high temperature operation results in cost disadvantages, including the expensive tubular reformer and large energy consumption [4]. The most common catalyst used for MSR is nickel, supported on ceramic oxides or oxides stabilized by hydraulic cement. Although other group VIII metals are active, they have some disadvantages: iron, for example, is rapidly oxidized, cobalt cannot withstand the partial pressures of steam, and the precious metals (rhodium, ruthenium, platinum, and palladium) are too expensive for commercial operation. The commonly used supports include  $\alpha$ -alumina, magnesia, calcium aluminate, or magnesium aluminate.

As said, MSR is a highly energy-intensive process, and alternative processes to produce synthesis gas include partial oxidation, dry reforming, and auto-thermal reforming. Among these alternatives, the catalytic partial oxidation to produce synthesis gas from methane (CPOM) is more energy efficient, since it has fast kinetics and is exothermic, thus avoiding the need of large reactors and large amounts of superheated steam [5]. Moreover, the stoichiometry of the partial oxidation (Equation (3)) produces a synthesis gas with an H<sub>2</sub>/CO ratio of 2:1, which enables its direct utilization for methanol or Fischer–Tropsch synthesis without additional adjustment.



Nickel is one of the most widely used active phases for CPOM, being supported on different oxide substrates (Al<sub>2</sub>O<sub>3</sub>, CeO<sub>2</sub>, La<sub>2</sub>O<sub>3</sub>, MgO, and ZrO<sub>2</sub>) [3].

Hydrogen production from dry reforming of methane has attracted considerable attention in recent years [6], due to the capability of the process to use two green-house gases (CO<sub>2</sub> and CH<sub>4</sub>, Equation (4)) to generate valuable feed-stocks with a more desirable H<sub>2</sub>/CO for the Fischer–Tropsch synthesis or methanol synthesis to gain highly-valuable chemical products.



Nickel catalysts possessing reasonably high catalytic activity and cheap cost have been widely used in methane dry reforming, being supported on many metal oxides, such as Al<sub>2</sub>O<sub>3</sub>, MgO, CeO<sub>2</sub>, or La<sub>2</sub>O<sub>3</sub> [7]. As reported, Ni-based catalysts in dry reforming are prone to sintering at high temperature and suffering from carbon deposition, which might result in their deactivation during the reaction. Several studies have demonstrated that the threshold nickel nanoparticle size affects the carbon formation, for non-noble metals, in fact, the rate of methane dissociation exceeds the rate of the oxidation bringing to the carbon formation on the metal as filaments. The rate of carbon formation is proportional to the nickel particle size, hence, for a size below 2 nm, the carbon formation significantly slows down [8]. In the literature, different methods were proposed to suppress the sintering of nickel nanoparticles and carbon deposition, including the use of anatase TiO<sub>2</sub> nanosheets with high-energy (001) facets [7] or dealuminated FAU type Y and BEA zeolites [9] as support, or improving the dispersion of active metal nanoparticles [10], thus adding promoters [11]. Some researchers proposed catalysts novel configurations, including Ni-vanadate oxides nanostructures [12], microchannel reactor with thin films of Ni/Al<sub>2</sub>O<sub>3</sub> that were coated on stainless steel [13], or Titanium nitride (TiN) promoted nickel catalysts [14].

Autothermal methane reforming (ATR) is an important process for generating synthesis gas (syngas), which is a combination gas of CO and H<sub>2</sub>, through the combination of adiabatic steam reforming and non-catalytic partial oxidation [15]. Ni catalysts are used for this process, but they encounter the activity loss by sintering and coke formation and deposition, so they must be supported on metal oxides, such as CeO<sub>2</sub> [15].

This short review focused on the steam reforming process. The complexity of the traditional steam reforming process that involves many very different operation units is optimized for the industrial scale, limiting the possibility to realize a process intensification. In the last decade, the scientific research focused on the development of innovative hydrogen production systems as well as the optimization of the conventional processes and, in this sense, the catalyst has a fundamental role. In general, steam reforming catalysts must meet stringent requirements, such as high activity, reasonable life, good heat transfer, low pressure drop, high thermal stability, and excellent mechanical strength. In addition, the necessity of reducing the costs made the development of methane steam reforming processes operating at low temperature mandatory, so avoiding, for example, the use of special steel alloy. The development of new catalysts with well-defined properties is fundamental in order to reach this objective: in fact, the catalyst must activate methane at low temperature, it must drive its conversion up to equilibrium values at short contact times, and, in addition, it must be resistant to deactivation factors (including carbon formation, which is favored at low temperature, and preferential oxidation, which occurs at low temperature mainly for Ni catalysts) [1].

The literature is rich of papers concerning the performance of catalysts in methane steam reforming. Accordingly, this short review has the aim of giving an overview on the most recent advances (from 2015 up to now) in Ni based catalysts for methane steam reforming, while also considering the innovative structured catalysts that have been studied.

## 2. Ni Based Powder Catalysts

In this section, a short overview of recent articles on the use of unstructured catalysts is provided. In Section 2.1, the works monometallic Ni/support type are reported (Table 1), while in Section 2.2, the works on polymetallic Ni-Mx/support type are reported (Table 2), where Mx is a generic symbol indicating one or more additional metals or metal oxides. The Sections 2.3 and 2.4 are devoted to specific works on deactivation and simulation and kinetic studies.

### 2.1. Monometallic Catalysts

Ali et al. developed a nickel nanoparticle-based catalyst, by dispersing the Ni-nanoparticles on silica/alumina support; the resulting Ni/SiO<sub>2</sub>Al<sub>2</sub>O<sub>3</sub> catalyst showed good thermal stability, hydrogen selectivity, and coke resistance [16]. The performance of this catalyst, in methane steam reforming reaction (MSR), was also compared to those of a catalyst that was obtained by wet impregnation, with the same chemical composition. The nickel nanoparticle-based catalyst showed higher CH<sub>4</sub> conversion than the conventionally prepared catalyst, for all the studied temperatures; moreover, the time on stream test showed the excellent stability of the former. The better performance was attributed to the difference in the physicochemical properties; the nickel-based nanoparticle catalyst was characterized by smaller particle size, better dispersion, and reducibility of the active species. Katheria et al. studied the effect of calcination temperature on the stability and activity of Ni/MgAl<sub>2</sub>O<sub>4</sub> catalyst in MSR [17]. The results showed that the catalytic activity increases with the calcination temperature till 850 °C and decreases with a further increase of the temperature. This trend was related to the extension of the metal oxide support solid solution formation and anchoring of the nickel to the support, which increases with the calcination temperature, until 850 °C. The decrease of the activity of the catalyst calcined at 1000 °C was attributed to the formation of nickel aluminate. The stability of the catalysts was also related to the pressure; in general, the increase in pressure from 1 to 10-bar resulted in a decrease in stability, while an increase of the calcination temperature resulted in a decrease of the deactivation rate, due to a decreasing of the mean nickel crystallite size. Rogers et al. reported the preparation of nickel aluminate catalysts [18] by means of Pechini synthesis [19], with the compositions NiAl<sub>4</sub>O<sub>7</sub>, NiAl<sub>2</sub>O<sub>4</sub>, and Ni<sub>2</sub>Al<sub>2</sub>O<sub>5</sub> for dry reforming and the steam reforming of methane. In the Pechini method, the metal precursors are incorporated into the polymeric resin, which reduces differences in the chemical reactivity of the metal ions during the oxide formation, thus minimizing the mixed oxide segregation. The study revealed that reduced NiAl<sub>2</sub>O<sub>4</sub> and unreduced/reduced

$\text{Ni}_2\text{Al}_2\text{O}_5$  show high and stable activity in MSR and the nickel particles were identified as the active specie. Khani et al. published the results a work in which the activity in DRM, SRM and combined DRM/SRM of three  $\text{M}/\text{ZnLaAlO}_4$  ( $\text{M} = 10\%\text{Ni}, 3\%\text{Pt}, 3\%\text{Ru}$ ) nanocatalysts and  $10\%\text{Ni}/\gamma\text{-Al}_2\text{O}_3$  were compared [20]. The support was obtained by means of the gel combustion technique, while the catalysts were obtained by means of wet impregnation. The FE-SEM and TEM analysis revealed the nanometric structure of the supports. The MSR catalytic activity tests highlighted the best performance of  $3\%\text{Ru}/\text{ZnLaAlO}_4$ , both in terms of  $\text{CH}_4$  conversion and coke formation. Fang et al. showed the effect of the preparation method of the  $\text{Y}_2\text{Zr}_2\text{O}_7$  support on the activity of  $\text{Ni}/\text{Y}_2\text{Zr}_2\text{O}_7$  in the MSR reaction [21]. The  $\text{Y}_2\text{Zr}_2\text{O}_7$  pyrochlore supports were prepared by co-precipitation (CP), glycine-nitrate combustion (GNC) and hydrothermal (HT) methods and impregnated with nickel nitrate to prepare the three catalysts. The characterization results revealed that the hydrothermal method provided the highest surface area, while the co-precipitation provided the lowest one. The  $\text{H}_2$ -TPR results showed a stronger interaction of nickel with the glycine-nitrate combustion derivate support than with the other two; moreover, this catalyst showed the highest activity and stability in a time on stream test at  $800\text{ }^\circ\text{C}$  and 20 atm for 200 h. Thalinger et al. studied the effects of the metal-support interaction, in two Ni/perovskite catalysts ( $\text{Ni-La}_{0.6}\text{Sr}_{0.4}\text{FeO}_{3-\delta}$ ,  $\text{Ni-SrTi}_{0.7}\text{Fe}_{0.3}\text{O}_{3-\delta}$ , in methane steam reforming and methanation reaction [22]. The catalysts reduction in hydrogen treatment caused the Ni-Fe alloy formation, which is related to the reducibility of the perovskite and much more pronounced with lanthanum-based support. The higher the degree of reducibility of the support, the higher the degree of formation of the Ni-Fe alloy. A comparison of the catalytic activity of these catalysts, with respect to a  $\text{Ni}/\text{Al}_2\text{O}_3$  reference catalyst, in methane steam reforming, showed similar behavior between the latter and  $\text{Ni-SrTi}_{0.7}\text{Fe}_{0.3}\text{O}_{3-\delta}$ , which is characterized by a less degree of alloy formation. On the contrary, the  $\text{Ni-La}_{0.6}\text{Sr}_{0.4}\text{FeO}_{3-\delta}$  catalyst showed a suppressed catalytic performance. Yoo et al. studied the effect of the butyric acid in the preparation of  $\text{Ni}/\gamma\text{-Al}_2\text{O}_3$  catalysts for steam reforming of natural gas, containing 92 vol % of methane and 8 vol% of ethane [23]. The catalysts were obtained by the impregnation of alumina with a nickel nitrate solution, to which was previously dropped butyric acid, in a molar ratio Ni/butyric acid 0–1. All of the prepared catalysts showed a mesoporous structure and they contained a nickel aluminate phase; the nickel dispersion was related to the amount of butyric acid that was used in the preparation, and the higher dispersion was related to the higher methane adsorption capacity. The best performance, in terms of natural gas conversion and hydrogen yield, were obtained with the catalyst that was prepared with a molar ratio Ni/butyric acid of 0.25. Iglesias et al. reported a comparative study on nickel-based catalysts that were supported on ceria and ceria doped with 5 wt % of Zr, Pr or La [24]. The catalysts were obtained by coprecipitation by means of the urea method, and then calcined at three different temperatures (600, 750, and  $900\text{ }^\circ\text{C}$ ). All of the doped catalysts showed a higher oxygen mobility; the Zr-doped showed the highest oxygen mobility and nickel availability. The catalysts calcined at  $600\text{ }^\circ\text{C}$  were tested at  $600\text{ }^\circ\text{C}$  with a water/methane ratio below 3; all of the doped catalysts showed a lower deactivation with respect to the pure ceria supported catalyst, Zr-doped showed the best performance both with a water/methane ratio of 0.5, to which the hydrogen yield was 23%, and with a water/methane ratio of 3, to which the hydrogen yield was 70%. The catalysts that were calcined at  $750\text{ }^\circ\text{C}$  showed the highest methane conversion in all cases. The catalysts that were calcined at  $900\text{ }^\circ\text{C}$  were tested with a water/methane ratio 1 at 600, 700, and  $900\text{ }^\circ\text{C}$  showing higher deactivation with respect to ones calcined at  $600\text{ }^\circ\text{C}$ . Aghayan et al. reported the preparation of a one-dimensional nickel-based catalysts, by template assisted wet-combustion synthesis, for methane steam reforming and methanation reactions [25]. The catalysts were prepared by the infiltration of nickel nitrate and glycine solution in the blocks of nanofibers of mesoporous self-oriented  $\gamma$ -alumina, and subsequent calcined at  $400\text{ }^\circ\text{C}$  for 30 min. The NiO average particle size was 4 nm, while the alumina surface was covered with the  $\text{NiAl}_2\text{O}_4$  nanolayer. The catalysts showed outstanding activity and stability in methane steam reforming.

Park et al. reported the preparation of nickel nanoparticles that were supported on  $\text{Ni}_{0.4}\text{Mg}_{0.6}\text{O}$  solid solution, by the exsolution method, as catalysts for methane steam reforming [26]. The nickel

magnesium solid solution was prepared by the co-precipitation method, while the nickel nanoparticles were obtained during the reduction, with hydrogen, of the solid solution. The activity tests showed a good stability of the catalysts in 1000 h of time on stream. Zhang et al. reported a comparative study on the use of Ni-based catalysts that were supported on  $Y_2B_2O_7$  compounds, in which B was Ti, Sn, Zr, or Ce [27]. The supports were prepared by the coprecipitation method; the ratio between the radius of yttria and the metal ion designed as B decreases with series Ti, Sn, Zr, and Ce, as a consequence the crystalline structure become increasingly more disordered. The XPS analysis showed that on the surface of  $Ni/Y_2Ti_2O_7$  and  $Ni/Y_2Ce_2O_7$ , the more abundant active oxygen species are present, being beneficial to the removal of the carbonaceous deposits and keeping the nickel sites free from coking. The  $H_2$ -TPR results showed that the active sites have stronger interaction with the support, in  $Ni/Y_2Ti_2O_7$  and  $Ni/Y_2Sn_2O_7$  catalysts, resulting in catalysts with higher metallic surface area and better thermal stability. Moreover, the reduction of  $Ni/Y_2Sn_2O_7$  catalyst produced the  $Ni_3Sn_2$  alloy, which improved the coking resistance but depressed the activity. Finally, the catalysts were tested in methane steam reforming and methane dry reforming, and the  $Ni/Y_2Ti_2O_7$  catalyst showed the highest activity, stability, and the strongest coking resistance. Chen et al. studied  $mNi/xLa-Si$  ( $m = 7.5, 12.5, 15, 17.5, 22.5$ ) ( $x = 0, 1, 2, 3, 5, 7$ ) catalysts with a different weight percentage of nickel and lanthanum in a combined carbon dioxide and steam reforming of the methane reaction [28]. The catalysts were prepared via one-step hydrolysis and the condensation of tetraethoxysilane and the inorganic metal salt precursors with the assistance of poly(ethylene glycol) ( $M_{av} = 1000$ ) and ethylene glycol in a water solution of nitric acid. Moreover for a comparison a series of catalysts, with a nickel loading of 17.5% and a lanthanum/silicon ratio of 3, were prepared without the assistance of both poly(ethylene glycol) and ethylene glycol, and a catalyst with a nickel loading of 17.5% and a lanthanum/silicon ratio of 3, was prepared by the incipient impregnation method. The results showed that the addition of lanthanum had a beneficial effect on the catalytic activity. The catalysts that were prepared with the poly(ethylene glycol) and ethylene glycol assistance, with a nickel loading of 17.5%, showed an increase of the  $CH_4$  conversion with the lanthanum/silicon ratio, from 0 to 3, and a decreased with the lanthanum/silicon ratio, from 3 to 7. Moreover, the  $CH_4$  conversion, in the case of the catalyst that was prepared by impregnation, with a nickel loading of 17.5% and a lanthanum/silicon ratio, of 3, showed the lowest  $CH_4$  conversion. These results were related to the nickel particle sizes, thus an increase of the particle sizes correspond to a lowest  $CH_4$  conversion. A further comparison between these catalysts was also carried out, in terms of TOFs, calculated based on the initial  $CH_4$  conversions at 800 °C and a number of nickel surface per gram of catalyst, obtaining a same trend obtained with the  $CH_4$  conversion. The time on stream tests showed that the deactivation rate for both  $CO_2$  and  $CH_4$  decreased with the increase in La content in the lanthanum/silicon ratio of 0–3, while the deactivation rates increased for higher ratios. The effect of the different preparation route was also studied; the results showed that catalysts that were prepared with the poly(ethylene glycol) and ethylene glycol assistance showed the best performance, in terms of stability. The effect of the nickel loading on the catalytic activity showed that the  $CH_4$  conversion and the stability of the catalyst increased from 7.5 to 17.5 of Ni wt %, a further increase to 22.5 wt % did not significantly affect the  $CH_4$  conversion. The spent catalysts were analyzed by means of X-RAY Diffraction (XRD), Transmission Electron Microscopy (TEM), and Thermo Gravimetric analysis (TGA); the results showed an increase of the nickel particle size and coke formation for all of the catalysts and highlighted the effect of lanthanum promotion. The crystallite sizes and the coke amount that were recovered by TGA decreased with the lanthanum/silicon ratio from 0 to 3 and increased with the lanthanum/silicon ratio from 3 to 7. These results demonstrated that the catalyst that was prepared with the assistance of poly (ethylene glycol) and ethylene glycol had the best catalytic activity, stability, and coke resistance. Fang et al. studied the effect of rare earth element on the physicochemical properties of the  $Ni/Ln_2Ti_2O_7$  ( $Ln = La, Pr, Sm, \text{ and } Y$ ) catalysts for methane steam reforming [29]. The supports were prepared by the co-precipitation method, while the catalysts were prepared by impregnation and incipient wetness impregnation methods. The characterization results showed that changing the element from La and Pr to Sm and Y, the supports transformed from monoclinic layered

perovskite to monoclinic layered pyrochlore structure. The Ni active site resulted in being highly dispersed on the pyrochlore supports; moreover, a stronger interaction with the supports was also found; the amount of oxygen vacancies was higher for the pyrochlore supports, thus these catalysts exhibited higher catalytic activity. Among the studied catalysts, the Ni/Y<sub>2</sub>Ti<sub>2</sub>O<sub>7</sub> catalyst exhibited the highest catalytic activity and the best coke-resistance. Iglesias et al. studied the nickel catalysts that were supported on zirconium-doped ceria in the methane steam reforming reaction [30]. The supports were prepared by the coprecipitation method obtaining a solid solution with formula Ce<sub>1-x</sub>Zr<sub>x</sub>O<sub>2-δ</sub>, in which x was varied from 0 to 35%, while the catalysts were obtained by impregnation. The addition of zirconium enhanced the reducibility of the support and metallic dispersion, but diminished the specific surface area; however, the nickel area was maximized at a zirconium content of 15%. The effect of the nickel loading was also investigated, showing that the best performance was obtained with a loading of 5 wt %, to which the highest metallic surface area corresponded. These results were also confirmed in further studies that were reported from the same group [31]. Sebai et al. studied the use of ammonia, ethylamine, diethyl amine, and triethylamine, as ligands to complex nickel nitrate salt, in the preparation of 5 wt % NiO/γ-Al<sub>2</sub>O<sub>3</sub> catalysts for methane steam reforming [32]. The catalysts were prepared by incipient wetness impregnation of γ-Al<sub>2</sub>O<sub>3</sub>, via Ni-amines intermediate in-situ complexes formation. The results showed that the use of the amines complexation reduced the spinel phase formation; moreover, to a larger size of the Ni-amine complex, corresponded to a wider contact area with the support, leading to larger spacing between the resulting nickel particle, which was obtained after the calcination, thus preventing the agglomeration and enhancing the dissociative adsorption of CH<sub>x</sub> species. Dan et al. reported a study on two alumina supported nickel catalysts, with different pore sizes, 5.4 and 9.0 nm, which were tested in the combined steam and dry reforming of methane [33]. The results showed that the Ni/Al<sub>2</sub>O<sub>3</sub> catalyst with larger pore size was characterized by higher surface area, lower nickel crystallite sizes, higher proportion of stronger catalytic sites for hydrogen adsorption, and higher CO<sub>2</sub> adsorption capacity.

## 2.2. Polymetallic Catalysts, Promoters

Nickel-based catalysts, although widely used in reforming processes, are less active than noble metal-based catalysts and more prone to deactivation [1]. An effective strategy for improving the performance of the nickel-based catalysts resides in the use of promoters [34]. Carbon formation can be avoided when the CO<sub>2</sub> concentration in nickel crystals is lower than that at the equilibrium, hence decreasing the steady state carbon activity, which is achievable by enhancing the adsorption of steam or CO<sub>2</sub>, enhancing the rate of the surface reaction, or decreasing the rate and degree of methane activation and dissociation [35]. The use of promoters, which can improve the coke resistance of nickel-based catalysts in reforming processes, is a possible way to achieve these effects [36]. Promoters can also affect the reducibility and dispersion of nickel particles, by acting as structural promoters [37] as well as affecting the segregation in oxidation-reduction processes [38]. The promoters are usually metallic ions added to the active components, which can induce electronic changes or crystal structure modification [39]. In this section, a selection of the latest work on the effect of adding one or more metals to nickel-based catalysts, in methane steam reforming reaction, is provided.

Morales-Cano et al. studied the role of Rh, Ir, and Ru as promoters in Ni/α-Al<sub>2</sub>O<sub>3</sub> catalysts in the methane steam reforming reaction [40]. The sintering of the metal nanoparticles and the alloying between nickel and the metal promoters was realized by ageing at 800 °C and a P<sub>H<sub>2</sub>O</sub> = 22 bar. The characterization results revealed that the degree of alloying and sintering is strongly affected from the promoter. Rhodium and iridium showed an increase of the alloying degree with nickel during the ageing process, due to the high mobility of the nickel species and diffusion into the structure of the promoters; moreover, the sintering of the nickel particle was mitigated. Ruthenium showed a low propensity to alloy with nickel and, therefore, a lower sintering resistance was obtained. The density functional theory calculations showed that the diffusion of nickel atoms in ruthenium lattice structure is not energetically favorable; on the contrary, nickel atoms are equally stable in the first and second

surface layers of iridium and rhodium. The catalytic activity tests showed considerably higher activity for all of the bimetallic catalysts, Ni–Rh/Al<sub>2</sub>O<sub>3</sub>, Ni–Ir/Al<sub>2</sub>O<sub>3</sub> and Ni–Ru/Al<sub>2</sub>O<sub>3</sub>, than Ni/Al<sub>2</sub>O<sub>3</sub> in methane steam reforming reaction; moreover, the Ni–Rh/Al<sub>2</sub>O<sub>3</sub> and Ni–Ir/Al<sub>2</sub>O<sub>3</sub> showed higher activity than Ni–Rh/Al<sub>2</sub>O<sub>3</sub> and Ni–Ir/Al<sub>2</sub>O<sub>3</sub>, respectively; on the contrary, Ni–Ru/Al<sub>2</sub>O<sub>3</sub> showed lower activity than the monometallic Ru/Al<sub>2</sub>O<sub>3</sub>.

Lertwittayanon et al. studied the effect of CaZrO<sub>3</sub> as promoter for Ni/α-Al<sub>2</sub>O<sub>3</sub> catalysts in methane steam reforming [41]. The promoted catalysts were prepared by the impregnation of α-Al<sub>2</sub>O<sub>3</sub> with the mixed solution of calcium and zirconium nitrate; the resulting oxide was impregnated with the nickel nitrate solution. Each catalyst contained 10 wt % of nickel and 5, 10, or 15 wt % of CaZrO<sub>3</sub>. The activity tests highlighted the best performance of catalyst that was promoted with 15wt % of CaZrO<sub>3</sub>, in terms of CH<sub>4</sub> conversion and hydrogen yield. Three different S/C ratios were investigated (from 1/3 to 3); contrary to what was expected the S/C ratio 3 resulted in an excessive steam adsorption at the oxygen vacancies of the promoter; consequently, the competitive adsorption between methane and steam caused a decreasing of methane dissociation.

Jaiswar et al. studied the effect of the addition of platinum to Ni/MgAl<sub>2</sub>O<sub>4</sub> catalyst, in the MSR reaction [42]. The bimetallic catalysts were obtained by the dry impregnation of Ni/MgAl<sub>2</sub>O<sub>4</sub> with H<sub>2</sub>PtCl<sub>6</sub>·6H<sub>2</sub>O; a series of catalysts were prepared with a platinum percentage in the range 0–1 wt %. The results showed that the addition of platinum increased the activity of the catalyst and the highest effect was obtained by loading 0.1wt % of platinum, an increasing of the loading resulted in a decreasing of the activity. These results were related to metal dispersion, the highest dispersion was, in fact, obtained with 0.1 wt % loading of platinum. Azancot et al. studied the effect of the preparation method of Ni–Mg–Al based catalysts on the activity in methane steam reforming [43]. The catalysts were prepared by means of three techniques, for the impregnation of γ-alumina with magnesium nitrate and nickel nitrate, for the coprecipitation-impregnation method, in which the magnesium and aluminum nitrates were coprecipitated and, subsequently, impregnated with nickel nitrate, finally for coprecipitation of the three metal nitrates. The activity of the catalysts was related to the degree of Ni–Mg–Al interaction; according to the reducibility, the Ni/MgAl<sub>2</sub>O<sub>4</sub> catalyst showed the optimal metal-support interaction and the highest catalytic activity and hydrogen production. Boudjeloud et al. studied the La-doped nickel catalysts that were supported on α-Al<sub>2</sub>O<sub>3</sub>, at different Ni/La ratio (7/3, 8/2, 9/1) in methane steam reforming [44]. The results showed that the addition of lanthanum might cause strong change at the surface of NiO sites, obtaining smaller and better dispersed NiO particles with a strong interaction with the support, and increasing the spacing between the active nickel particles, thus preventing their agglomeration and sintering. The small Ni particles, which were highly dispersed, enhanced the dissociative adsorption of CH<sub>x</sub> species, while the highest hydrogen yield was obtained with the 7Ni-3La/α-Al<sub>2</sub>O<sub>3</sub> catalyst. Nazari and Alavi studied the effect of adding copper and zinc to Ni/Al<sub>2</sub>O<sub>3</sub> catalysts for methane steam reforming reaction [45]. The results showed that zinc could enhance the activity, stability, and hydrogen selectivity of the Ni/Al<sub>2</sub>O<sub>3</sub> catalysts; copper led to a significant enhancement in the stabilization of the catalyst toward the coke formation. Based on the Taguchi design results, the optimum catalyst, in terms of hydrogen yield and lower selectivity to CO, was 15Ni-1Cu-5Zn/γ-Al<sub>2</sub>O<sub>3</sub>.

**Table 1.** Summary of preparation procedures and operative conditions used in monometallic catalysts and related publications.

Catalysts (Particle Size)	Preparation Procedure	Operative Conditions MSR	Selected Catalyst CH <sub>4</sub> conv./vol % Versus Temperature/Pressure (Time on Stream, Deactivation)	Ref.
Ni/SiO <sub>2</sub> Al <sub>2</sub> O <sub>3</sub> (5–8 ± 1.2 nm)	10 wt % SiO <sub>2</sub> Al <sub>2</sub> O <sub>3</sub> , NiCl <sub>2</sub> *6H <sub>2</sub> O, NaOH, ethylene glycol, N <sub>2</sub> H <sub>4</sub> *H <sub>2</sub> O. T = 90 °C. T <sub>calcination</sub> = 900 °C.	WHSV = 1700 mL/g*h, CH <sub>4</sub> /H <sub>2</sub> O = 1, T = 650–900 °C.	X <sub>CH<sub>4</sub></sub> ≈ 100%, T = 750 °C, P = 1-bar (50 h, 0.41%)	[16]
Ni/SiO <sub>2</sub> Al <sub>2</sub> O <sub>3</sub> (18–20 ± 3.1 nm)	10 wt % SiO <sub>2</sub> Al <sub>2</sub> O <sub>3</sub> , Ni(NO <sub>3</sub> ) <sub>2</sub> *6H <sub>2</sub> O, H <sub>2</sub> O. T <sub>calcination</sub> = 900 °C.	WHSV = 1700 mL/g*h; CH <sub>4</sub> /H <sub>2</sub> O = 1; T = 650–900 °C.	X <sub>CH<sub>4</sub></sub> ≈ 75%, T = 750 °C, P = 1-bar (50 h, 9.2%) X <sub>CH<sub>4</sub></sub> ≈ 100%, T = 900 °C, P = 1-bar	[16]
Ni/MgAl <sub>2</sub> O <sub>4</sub> (0.25–0.30 μm)	MgAl <sub>2</sub> O <sub>4</sub> , Ni(NO <sub>3</sub> ) <sub>2</sub> *6H <sub>2</sub> O, H <sub>2</sub> O. T <sub>calcination</sub> = 350 °C, 500 °C, 650 °C, 850 °C, 1000 °C.	WHSV = 0.34 g <sub>cat</sub> /h/mol; CH <sub>4</sub> /H <sub>2</sub> O/N <sub>2</sub> = 1/5/1; T = 600 °C; P = 1–10-bar	X <sub>CH<sub>4</sub></sub> = 40–50%, T = 600 °C, P = 1-bar X <sub>CH<sub>4</sub></sub> = 35–45%, T = 600 °C, P = 5-bar X <sub>CH<sub>4</sub></sub> = 35–45%, T = 600 °C, P = 10-bar	[17]
NiAl <sub>4</sub> O <sub>7</sub> (8–10 nm), NiAl <sub>2</sub> O <sub>4</sub> (6–7 nm), Ni <sub>2</sub> Al <sub>2</sub> O <sub>5</sub> (3–4 nm)	Ni(NO <sub>3</sub> ) <sub>2</sub> *6H <sub>2</sub> O, Al(NO <sub>3</sub> ) <sub>3</sub> *9H <sub>2</sub> O, ethylene glycol, citric acid, H <sub>2</sub> O. T <sub>calcination</sub> = 1000 °C.	GHSV = 65,500 h <sup>-1</sup> ; H <sub>2</sub> O/CH <sub>4</sub> /N <sub>2</sub> = 2.4/1/3.4; T = 700 °C; P = 1-bar	NiAl <sub>4</sub> O <sub>7</sub> not active NiAl <sub>2</sub> O <sub>4</sub> X <sub>CH<sub>4</sub></sub> = 78%, T = 700 °C; P = 1 bar (12 h, 2%) Ni <sub>2</sub> Al <sub>2</sub> O <sub>5</sub> X <sub>CH<sub>4</sub></sub> = 82 %, T = 700 °C, P = 1 bar (12 h, 7%)	[18]
Ni/ZnLaAlO <sub>4</sub> (50–60 nm) Pt/ZnLaAlO <sub>4</sub> (50–60 nm) Ru/ZnLaAlO <sub>4</sub> (≈40 nm) Ni/γ-Al <sub>2</sub> O <sub>3</sub> (50–60 nm)	Ni(NO <sub>3</sub> ) <sub>2</sub> *6H <sub>2</sub> O or H <sub>2</sub> PtCl <sub>6</sub> *6H <sub>2</sub> O or Ru(N=O)(NO <sub>3</sub> ) <sub>3</sub> , ZnLaAlO <sub>4</sub> or γ-Al <sub>2</sub> O <sub>3</sub> , H <sub>2</sub> O. T <sub>calcination</sub> = 700 °C.	GHSV = 3500,7000 and 10,500 h <sup>-1</sup> ; H <sub>2</sub> O/CH <sub>4</sub> /Ar = 3/1/3; T = 600–800 °C; P = 1 bar	Ni/ZnLaAlO <sub>4</sub> X <sub>CH<sub>4</sub></sub> ≈ 72%, T = 700 °C, P = 1 bar (10,500 h <sup>-1</sup> , 30 h, ≈8%) Pt/ZnLaAlO <sub>4</sub> , X <sub>CH<sub>4</sub></sub> ≈ 88% X <sub>CH<sub>4</sub></sub> ≈ 72%, T = 700 °C, P = 1 bar (10,500 h <sup>-1</sup> , 30 h, ≈1%) Ru/ZnLaAlO <sub>4</sub> X <sub>CH<sub>4</sub></sub> ≈ 98%, T = 700 °C, P = 1 bar (10,500 h <sup>-1</sup> , 30 h, ≈0%)	[20]

Table 1. Cont.

Catalysts (Particle Size)	Preparation Procedure	Operative Conditions MSR	Selected Catalyst CH <sub>4</sub> conv./vol % Versus Temperature/Pressure (Time on Stream, Deactivation)	Ref.
Ni/Y <sub>2</sub> Zr <sub>2</sub> O <sub>7-x</sub> x = HT, CP, GNC	Ni(NO <sub>3</sub> ) <sub>2</sub> *6H <sub>2</sub> O, Y <sub>2</sub> Zr <sub>2</sub> O <sub>7-x</sub> , H <sub>2</sub> O. T <sub>calcination</sub> = 800 °C. x = HT, CP, GNC	WHSV = 72,000 mL/h gcat; H <sub>2</sub> O/CH <sub>4</sub> = 2/1; T = 550–800 °C; P = 1, 20 atm	Ni/Y <sub>2</sub> Zr <sub>2</sub> O <sub>7-HT</sub> X <sub>CH<sub>4</sub></sub> ≈ 83%, T = 800 °C, P = 1 atm (100 h, 11%) Ni/Y <sub>2</sub> Zr <sub>2</sub> O <sub>7-CP</sub> X <sub>CH<sub>4</sub></sub> ≈ 60%, T = 800 °C, P = 1 atm (100 h, 15%) Ni/Y <sub>2</sub> Zr <sub>2</sub> O <sub>7-GNC</sub> X <sub>CH<sub>4</sub></sub> ≈ 98%, T = 800 °C, P = 1 atm (100 h, 0%)	[21]
Ni–La <sub>0.6</sub> Sr <sub>0.4</sub> FeO <sub>3-δ</sub> (50 nm) Ni–SrTi <sub>0.7</sub> Fe <sub>0.3</sub> O <sub>3-δ</sub> (25 nm)	Ni(acac) <sub>2</sub> , acetone, La <sub>0.6</sub> Sr <sub>0.4</sub> FeO <sub>3-δ</sub> or SrTi <sub>0.7</sub> Fe <sub>0.3</sub> O <sub>3-δ</sub> T <sub>calcination</sub> = 600 °C.	H <sub>2</sub> O/CH <sub>4</sub> = 1/1; T = 550–600 °C; P = 1 bar	Ni–SrTi <sub>0.7</sub> Fe <sub>0.3</sub> O <sub>3-δ</sub> X <sub>CH<sub>4</sub></sub> ≈ 90%, T = 600 °C, P = 1 bar	[22]
Ni/γ-Al <sub>2</sub> O <sub>3</sub> (<10 nm)	γ-Al <sub>2</sub> O <sub>3</sub> , H <sub>2</sub> O, Ni(NO <sub>3</sub> ) <sub>2</sub> *6H <sub>2</sub> O, butyric acid. Ni/butyric acid 0-1 T <sub>calcination</sub> = 700 °C.	Flow = Natural gas (92 vol % methane and 8 vol % ethane) 5 mL/min., steam (11 mL/min.), and nitrogen (18 mL/min.).	10Ni/γ-Al <sub>2</sub> O <sub>3</sub> Ni/butyric acid = 0.25 X <sub>natural gas</sub> ≈ 64%, T = 550 °C (1000 min, 0 %)	[23]
Ni/Ce <sub>0.95</sub> M <sub>0.05</sub> O <sub>2-d</sub> (M = Zr, Pr, La) (17–35 nm)	Ce <sub>0.95</sub> M <sub>0.05</sub> O <sub>2-d</sub> (M = Zr, Pr, La), H <sub>2</sub> O, Ni(NO <sub>3</sub> ) <sub>2</sub> *6H <sub>2</sub> O. T <sub>calcination</sub> = 600, 750, 900 °C.	Weight/Flow = 1 g min/Nml), CH <sub>4</sub> (12.5 %), H <sub>2</sub> O/CH <sub>4</sub> (0.5, 1, 1.5 or 3).	5% Ni/CeZr <sub>5</sub> X <sub>CH<sub>4</sub></sub> = 72%, T = 600 °C, R = 3. (4 h, ≈12%)	[24]
Ni/γ-Al <sub>2</sub> O <sub>3</sub> (<50 nm)	γ-Al <sub>2</sub> O <sub>3</sub> , H <sub>2</sub> O, Ni(NO <sub>3</sub> ) <sub>2</sub> *6H <sub>2</sub> O, glycine. T <sub>calcination</sub> = 400 °C	WHSV = 45,000–360,000 scm <sup>3</sup> g <sup>-1</sup> h <sup>-1</sup> , H <sub>2</sub> O/CH <sub>4</sub> = 2/1, T = 650 °C.	CH <sub>4</sub> ≈ 10% vol, H <sub>2</sub> ≈ 50% vol T = 650 °C (50 h, 0%)	[25]
Ni/Ni <sub>0.4</sub> Mg <sub>0.6</sub> O (18–28 nm)	Reduction of Ni <sub>0.4</sub> Mg <sub>0.6</sub> O with hydrogen.	WHSV = 15,800 cm <sup>3</sup> g <sup>-1</sup> h <sup>-1</sup> , H <sub>2</sub> O/CH <sub>4</sub> = 0.5.	X <sub>CH<sub>4</sub></sub> ≈ 99%, T = 800 °C. (100 h, 0%)	[26]

Table 1. Cont.

Catalysts (Particle Size)	Preparation Procedure	Operative Conditions MSR	Selected Catalyst CH <sub>4</sub> conv./vol % Versus Temperature/Pressure (Time on Stream, Deactivation)	Ref.
Ni/Y <sub>2</sub> B <sub>2</sub> O <sub>7</sub> (B = Ti, Sn, Zr, or Ce)	Ni(NO <sub>3</sub> ) <sub>2</sub> *6H <sub>2</sub> O, H <sub>2</sub> O, Y <sub>2</sub> B <sub>2</sub> O <sub>7</sub> (B = Ti, Sn, Zr, or Ce) T <sub>calcination</sub> = 800 °C.	WHSV = 36,000 mLh <sup>-1</sup> g <sub>cat</sub> <sup>-1</sup> , H <sub>2</sub> O/CH <sub>4</sub> = 2:1.	Ni/Y <sub>2</sub> Ti <sub>2</sub> O <sub>4</sub> X <sub>CH<sub>4</sub></sub> ≈ 85%, T = 750 °C (50 h, ≈ 5%) Ni/Y <sub>2</sub> Sn <sub>2</sub> O <sub>4</sub> X <sub>CH<sub>4</sub></sub> ≈ 9%, T = 750 °C (50 h, ≈ 2%) Ni/Y <sub>2</sub> Zr <sub>2</sub> O <sub>4</sub> X <sub>CH<sub>4</sub></sub> ≈ 43%, T = 750 °C (50 h, ≈ 35%) Ni/Y <sub>2</sub> Ce <sub>2</sub> O <sub>4</sub> X <sub>CH<sub>4</sub></sub> ≈ 65%, T = 750 °C (50 h, ≈ 5%)	[27]
mNi/xLa-Si (m = 7.5,12.5,15,17.5,22.5) (x = 0,1,0,2,0,3,0,5,0,7,0) (14–20 nm)	Ni(NO <sub>3</sub> ) <sub>2</sub> *6H <sub>2</sub> O, La(NO <sub>3</sub> ) <sub>3</sub> *6H <sub>2</sub> O, PEG, H <sub>2</sub> O, ethylene glycol, nitric acid, TEOS. T <sub>calcination</sub> = 800 °C.	GHSV = 1.584 × 10 <sup>5</sup> mL/g <sub>cat</sub> h, CH <sub>4</sub> /CO <sub>2</sub> /H <sub>2</sub> O = 1/0.4/0.8, T = 730–830 °C, P = 1 atm	17.5Ni/3.0La-Si X <sub>CH<sub>4</sub></sub> ≈ 85%, T = 800 °C (60 h, ≈ 5%)	[28]
Ni/Ln <sub>2</sub> Ti <sub>2</sub> O <sub>7</sub> (Ln = La, Pr, Sm, and Y) (16.6–17.5 nm)	Ni(NO <sub>3</sub> ) <sub>2</sub> *6H <sub>2</sub> O, H <sub>2</sub> O, Ln <sub>2</sub> Ti <sub>2</sub> O <sub>7</sub> (Ln = La, Pr, Sm, and Y). T <sub>calcination</sub> = 800 °C.	WHSV = 72,000 mL/gh, H <sub>2</sub> O/CH <sub>4</sub> = 2/1, T = 600–800 °C, P = 1 atm.	Ni/Y <sub>2</sub> Ti <sub>2</sub> O <sub>7</sub> X <sub>CH<sub>4</sub></sub> ≈ 85%, T = 800 °C (50 h, ≈ 5%)	[29]
yNi/Ce <sub>1-x</sub> Zr <sub>x</sub> O <sub>2-δ</sub> (X = 0, 0.15, y = 2,5,10).	Ni(NO <sub>3</sub> ) <sub>2</sub> *6H <sub>2</sub> O, H <sub>2</sub> O, Ce <sub>1-x</sub> Zr <sub>x</sub> O <sub>2-δ</sub> (X = 0, 0.15). T <sub>calcination</sub> = 600 °C.	τ = 1 mg min/Nml H <sub>2</sub> O/CH <sub>4</sub> = 1/1, T = 600 °C.	5Ni/Ce <sub>0.85</sub> Zr <sub>0.15</sub> O <sub>2-δ</sub> X <sub>CH<sub>4</sub></sub> ≈ 70%, T = 600 °C (4 h)	[30]
Ni/γ-Al <sub>2</sub> O <sub>3</sub> (11.4–14.2 nm)	γ-Al <sub>2</sub> O <sub>3</sub> , Ni(NO <sub>3</sub> ) <sub>2</sub> *6H <sub>2</sub> O, H <sub>2</sub> O, amine. Ni/Amine = 1/6, Amine = ammonia, ethylamine, diethylamine, triethylamine.	GHSV = 24 × 10 <sup>3</sup> mL/g <sub>cat</sub> h, H <sub>2</sub> O/CH <sub>4</sub> = 3/1, T = 500–800 °C,	5Ni/γ-Al <sub>2</sub> O <sub>3</sub> Amine = diethylamine X <sub>CH<sub>4</sub></sub> ≈ 90%, T = 700 °C (500 min, ≈ 0%)	[32]
Ni/Al <sub>2</sub> O <sub>3</sub> (6–12 nm)	Al <sub>2</sub> O <sub>3</sub> , Ni(NO <sub>3</sub> ) <sub>2</sub> *6H <sub>2</sub> O, H <sub>2</sub> O. T <sub>calcination</sub> = 550 °C.	GHSV = 100 mL/min., CH <sub>4</sub> /CO <sub>2</sub> = 1/0.48, H <sub>2</sub> O/CH <sub>4</sub> = 1.2/0.48, 3.5/0.48, 6.1/0.48. T = 600–700 °C.	10 wt % Ni/Al <sub>2</sub> O <sub>3</sub> , X <sub>CH<sub>4</sub></sub> ≈ 99%, T = 700 °C (20 h, ≈ 0%)	[33]

**Table 2.** Summary of preparation procedures and operative conditions used in polymetallic catalysts and related publications.

Catalyst (Particle Size)	Preparation Procedure	Operative Conditions	Selected Catalyst CH <sub>4</sub> conv./CH <sub>4</sub> conv. Rate Temperature/Pressure (Time on Stream, Deactivation)	Ref
Ni-X/ $\alpha$ -Al <sub>2</sub> O <sub>3</sub> X = Ru, Rh, Ir (7–30 nm)	$\alpha$ -Al <sub>2</sub> O <sub>3</sub> , Ni(NO <sub>3</sub> ) <sub>2</sub> *6H <sub>2</sub> O, H <sub>2</sub> O, Rh(NO <sub>3</sub> ) <sub>2</sub> *xH <sub>2</sub> O or IrCl <sub>3</sub> *6H <sub>2</sub> O or Ru(NO <sub>3</sub> ) <sub>3</sub> (NO). T <sub>calcination</sub> = 450 °C.	GHSV = 11,195 h <sup>-1</sup> ; CH <sub>4</sub> /H <sub>2</sub> O/H <sub>2</sub> = 2/8/0.8; T = 500 °C; P = 30 bar	Ni-Ir/ $\alpha$ -Al <sub>2</sub> O <sub>3</sub> CH <sub>4</sub> conv. Rate $\approx$ 0.17 mol/g <sub>cat</sub> *h Ni-Ru/ $\alpha$ -Al <sub>2</sub> O <sub>3</sub> CH <sub>4</sub> conv. rate $\approx$ 0.22 mol/g <sub>cat</sub> *h Ni-Rh/ $\alpha$ -Al <sub>2</sub> O <sub>3</sub> CH <sub>4</sub> conv. rate $\approx$ 0.22 mol/g <sub>cat</sub> *h	[40]
Ni/CaZrO <sub>3</sub> / $\alpha$ -Al <sub>2</sub> O <sub>3</sub> X = 5,10,15 wt %	$\alpha$ -Al <sub>2</sub> O <sub>3</sub> , H <sub>2</sub> O, Ca(NO <sub>3</sub> ) <sub>2</sub> *4H <sub>2</sub> O, ZrO(NO <sub>3</sub> ) <sub>2</sub> *H <sub>2</sub> O. T <sub>calcination</sub> = 800 °C. Ni(NO <sub>3</sub> ) <sub>2</sub> *6H <sub>2</sub> O, H <sub>2</sub> O. T <sub>calcination</sub> = 700 °C.	WHSV = 60,000 mL/h g; H <sub>2</sub> O/CH <sub>4</sub> /Ar = 1/1/3, 1/3/6 and 3/1/6.	15Ni/15CaZrO <sub>3</sub> / $\alpha$ -Al <sub>2</sub> O <sub>3</sub> XCH <sub>4</sub> $\approx$ 67%, T = 700 °C S/C = 1 (10 h, $\approx$ 0%)	[41]
xPt/15 wt %Ni/MgAl <sub>2</sub> O <sub>4</sub> x = 0–1 wt % (7.6–14.9 nm)	15 wt %Ni/MgAl <sub>2</sub> O <sub>4</sub> , H <sub>2</sub> PtCl <sub>6</sub> *6H <sub>2</sub> O, H <sub>2</sub> O. T <sub>calcination</sub> = 600 °C.	WHSV = 0.34 g <sub>cat</sub> *h/mol; CH <sub>4</sub> /H <sub>2</sub> O/N <sub>2</sub> = 1/5/1 T = 600 °C; P = 1–10 bar	T = 600 °C, P = 1 atm x = 0.00 wt % X <sub>CH<sub>4</sub></sub> $\approx$ 48% (8 h, $\approx$ 1%) x = 0.01 wt % X <sub>CH<sub>4</sub></sub> $\approx$ 50% (8 h, $\approx$ 2%) x = 0.05 wt % X <sub>CH<sub>4</sub></sub> $\approx$ 59% (8 h, $\approx$ 1%) x = 0.1 wt % X <sub>CH<sub>4</sub></sub> $\approx$ 62% (8 h, $\approx$ 1%) x = 0.3 wt % X <sub>CH<sub>4</sub></sub> $\approx$ 63% (8 h, $\approx$ 3%) x = 1.0 wt % X <sub>CH<sub>4</sub></sub> $\approx$ 19% (8 h, $\approx$ 2%)	[42]

Table 2. Cont.

Catalyst (Particle Size)	Preparation Procedure	Operative Conditions	Selected Catalyst CH <sub>4</sub> conv./CH <sub>4</sub> conv. Rate Temperature/Pressure (Time on Stream, Deactivation)	Ref
Ni/Mg/ $\gamma$ -Al <sub>2</sub> O <sub>3</sub> (21.9 nm)	1.Mg(NO <sub>3</sub> ) <sub>2</sub> *6H <sub>2</sub> O, $\gamma$ -Al <sub>2</sub> O <sub>3</sub> H <sub>2</sub> O. 2.Ni(NO <sub>3</sub> ) <sub>2</sub> *6H <sub>2</sub> O., Mg/ $\gamma$ -Al <sub>2</sub> O <sub>3</sub> H <sub>2</sub> O. T <sub>calcination</sub> = 550 °C.	GHSV = 60 L/gh, H <sub>2</sub> O/CH <sub>4</sub> = 1.24, T = 750–850 °C.	X <sub>CH<sub>4</sub></sub> $\approx$ 60%, T = 850 °C	[43]
Ni/MgAl <sub>2</sub> O <sub>4</sub> (14.9 nm)	1.Mg(NO <sub>3</sub> ) <sub>2</sub> *6H <sub>2</sub> O, Al(NO <sub>3</sub> ) <sub>3</sub> *9H <sub>2</sub> O, NaOH, Na <sub>2</sub> CO <sub>3</sub> , H <sub>2</sub> O. 2.Ni(NO <sub>3</sub> ) <sub>2</sub> *6H <sub>2</sub> O, MgAl <sub>2</sub> O <sub>4</sub> , H <sub>2</sub> O. T <sub>calcination</sub> = 900 °C.	GHSV = 60 L/gh, H <sub>2</sub> O/CH <sub>4</sub> = 1.24, T = 750–850 °C.	X <sub>CH<sub>4</sub></sub> $\approx$ 74%, T = 850 °C	[43]
NiMgAlO <sub>x</sub> (42.1 nm)	Mg(NO <sub>3</sub> ) <sub>2</sub> *6H <sub>2</sub> O, Al(NO <sub>3</sub> ) <sub>3</sub> *9H <sub>2</sub> O, Ni(NO <sub>3</sub> ) <sub>2</sub> *6H <sub>2</sub> O, NaOH, Na <sub>2</sub> CO <sub>3</sub> , H <sub>2</sub> O. T <sub>calcination</sub> = 550 °C.	GHSV = 60 L/gh, H <sub>2</sub> O/CH <sub>4</sub> = 1.24, T = 750–850 °C.	X <sub>CH<sub>4</sub></sub> $\approx$ 35%, T = 850 °C	[43]
xNi-yLa/ $\alpha$ -Al <sub>2</sub> O <sub>3</sub> (x/y = 7/3, 8/2, 9/1)	$\alpha$ -Al <sub>2</sub> O <sub>3</sub> , Ni(NO <sub>3</sub> ) <sub>2</sub> *6H <sub>2</sub> O, La(NO <sub>3</sub> ) <sub>3</sub> *6H <sub>2</sub> O, H <sub>2</sub> O. T <sub>calcination</sub> = 700 °C.	GHSV = 32 $\times$ 10 <sup>3</sup> mL/g <sub>cat</sub> h, CH <sub>4</sub> /H <sub>2</sub> O = 1/3, 10% CH <sub>4</sub> /Ar, T = 500–800 °C.	7Ni-3La/ $\alpha$ -Al <sub>2</sub> O <sub>3</sub> X <sub>CH<sub>4</sub></sub> $\approx$ 87%, T = 600 °C (12 h, $\approx$ 0%)	[44]
xNi-yCu-tZn/ $\gamma$ -Al <sub>2</sub> O <sub>3</sub> (x = 5,10,15; y = 1,3,5; t = 1,3,5)	$\gamma$ -Al <sub>2</sub> O <sub>3</sub> , Ni(NO <sub>3</sub> ) <sub>2</sub> *6H <sub>2</sub> O, Zn (NO <sub>3</sub> )*6H <sub>2</sub> O, Cu (NO <sub>3</sub> )*6H <sub>2</sub> O, H <sub>2</sub> O. T <sub>calcination</sub> = 900 °C.	Methane molar rate (mol/min.) = 0.0002719 H <sub>2</sub> O/CH <sub>4</sub> ratio = 4, T = 700°C.	15Ni-1Cu-5Zn/ $\gamma$ -Al <sub>2</sub> O <sub>3</sub> X <sub>CH<sub>4</sub></sub> $\approx$ 95%, T = 700 °C (10 h, $\approx$ 3%)	[45]

### 2.3. Deactivation Studies

Catalysts life is intimately dependent on the process conditions and the composition of the feed stream; a reliable prediction of the catalyst's life cycle is extremely difficult [46]. Deactivation, which can take place by sintering, thermal degradation, coking, and poisoning, is one of the major issues related to the use of nickel-based catalysts in reforming processes. Sintering is an agglomeration phenomenon, for which the crystallite growth of the catalytic phases or the loss of the surface area of the support occur. The thermal degradation is a chemical transformation of the catalytic phase to non-catalytic phases [47]. Coking is a phenomenon for which coke covers the catalytic surface as the result of side reactions, such as the Boudouard reaction or cracking. Poisoning is due to the strong chemisorption of species on catalytic sites that block the catalytic activity. Catalysts regeneration is intimately related to the type of deactivation, which is the most used way to regenerate the reforming catalysts involves oxidative environments at high temperatures to burn off the coke [48]. Nickel-based catalysts that are deactivated by particle sintering can be successful regenerated by treatment with oxidative CO<sub>2</sub> atmosphere, as well as catalysts, deactivated by sulfur poisoning can be regenerated by steam/hydrogen stream treatment [49]. In this section, a selection of the latest article in deactivation studies in methane steam reforming process is provided.

Jablonski et al. presented a comparative study on the deactivation by H<sub>2</sub>S, SO<sub>2</sub>, and COS of Ni/YSZ and Ni/K<sub>2</sub>O-CaAl<sub>2</sub>O<sub>4</sub> commercial catalysts, in methane steam and dry reforming [50]. The composition of the feed stream was: 14.3 vol % He, 8.6 vol % H<sub>2</sub>, 34.3 vol % N<sub>2</sub>, 14.3 vol % CH<sub>4</sub>, and 28.5 vol % H<sub>2</sub>O or CO<sub>2</sub>. The experiments were carried out, as follows: 30 min. of reforming followed by 90 min. of reforming in presence of sulphur species (H<sub>2</sub>S, SO<sub>2</sub>, and COS at concentrations of 1, 3, and 5 ppm). The results showed that the Ni/YSZ catalyst was less active than the Ni/K<sub>2</sub>O-CaAl<sub>2</sub>O<sub>4</sub> commercial catalyst and it was also more sensitive to sulphur poisoning. The deactivation rates trend for the sulphur species on both catalysts was COS > SO<sub>2</sub> ≥ H<sub>2</sub>S. Yang studied the deactivation behavior of a nickel-based catalyst by cofeeding H<sub>2</sub>S in the methane steam reforming reaction [51]. The catalyst was prepared by wet impregnation of cement-modified α-Al<sub>2</sub>O<sub>3</sub>, with the salt precursors of cerium and nickel. The steam reforming reaction was carried out at a steam to methane ratios of 3.0 with a CH<sub>4</sub> flow of 40 mL/min, and at the reaction temperature of 700 °C, 800 °C, and 900 °C. After reaching a reaction steady state, H<sub>2</sub>S was introduced into the reactor and the activity was evaluated every 30 min. The results showed that the sulfur is more strongly adsorbed at lower temperatures, while a faster deactivation, at constant temperature, occurs at a higher concentration of hydrogen sulfide. At 900 °C, the sulfur poisoned catalyst keeps a residual reforming activity, while at 700 °C the activity of the catalyst rapidly decreases even at very low hydrogen sulfide concentration. Three regenerating techniques were also studied, by treatment with steam, with air and steam, or with hydrogen and steam. Treating the catalysts with steam for three hours followed by treating with hydrogen for three hours can be utilized to achieve the regeneration; however, the extent of the regeneration was related to temperature and increased with the increase of the temperature.

Lafrune et al. studied the effect of exposure to naphthalene of Ni and Rh-based catalysts for MSR [52]. The preparation of the catalysts firstly provided the synthesis of the support; silicalite-1 was prepared by means of sol-gel method, while the Ni@silicalite-1 catalysts were prepared by means of an encapsulation method [53]. The reforming reactions were carried out at 700–900 °C at a space velocity GHSV of 750,000 h<sup>-1</sup>, by feeding a reformat stream gas. The results showed a strong decrease of the CH<sub>4</sub> conversion in the presence of 1400 ppm of naphthalene; however, the effect was partially reversible. The encapsulation did not prevent the poisoning of the catalysts, probably because naphthalene was able to hit the Nickel particles, despite the encapsulation. A similar deactivation was obtained with pyrene, which is bulkier, but cracks to naphthalene; on the contrary, the effect of toluene was negligible. Haynes et al. studied the effect of calcination temperature on Ni-based lanthanum zirconate pyrochlore catalysts for methane steam reforming [54]. The results showed that the catalysts that were calcined below 700 °C gave rise to the highest activity and selectivity, due to the smaller and well-dispersed nickel particles, and to less lanthanum enrichment on the surface of the

support. The catalysts that were calcined at 700–900 °C showed a reversible deactivation at both low and high reaction pressure ( $P = 1.8$  MPa), which suggests a synergistic interaction between nickel and lanthanum. The exposure of fresh catalysts to high reaction pressures leads to the rapid and irreversible deactivation, due to the presence of  $\text{LaO}_x$  species that cover the Ni particles. Hernandez et al. studied the effect of  $\text{H}_2\text{S}$  and thiophene on the methane and benzene steam reforming and water gas shift, for  $\text{Ni}/\text{Al}_2\text{O}_3$ ,  $\text{Ni}/\text{mayerite}$  and  $\text{Rh}/\text{Al}_2\text{O}_3$  catalysts [55]. The experiments were carried out by feeding a simulated coke oven gas stream, and the temperature range studied was 675–900 °C. The results showed that the temperature plays a crucial role in determining the poisoning of the catalysts, in particular decreasing the temperature leads to the poisoning effect increasing, due to the exothermicity of the sulfur chemisorption equilibrium. The thermal conversion of thiophene reached the 42% at 800 °C, and the main products were  $\text{H}_2\text{S}$  and  $\text{COS}$ . In the presence of thiophene,  $\text{Ni}/\text{Al}_2\text{O}_3$  and  $\text{Ni}/\text{mayerite}$  showed similar benzene steam reforming activity, while  $\text{Rh}/\text{Al}_2\text{O}_3$  outperformed both the nickel catalysts, especially at temperatures that were above 775 °C. The regeneration of the catalyst activity was only possible at 900 °C.

#### 2.4. Kinetics and Simulations

Turchetti et al. studied the reaction rate of low-temperature methane/biogas steam reforming on two Ni-based catalysts ( $\text{Ni-Pt}/\text{CeO}_2$  and  $\text{Ni}/\text{CeZrLa}$ ) [56]. The two catalysts were prepared by wet impregnation and the MSR experiments were carried out in the GHSV range of 20,000–70,000  $\text{h}^{-1}$ , temperature range 400–550 °C, pressure 1–7-bar,  $\text{H}_2\text{O}/\text{CH}_4 = 3/1$ . The estimated apparent activation energy was similar for the two catalysts,  $71.96 \pm 0.50$  and  $70.76 \pm 0.65$  kJ/mol for  $\text{Ni-Pt}/\text{CeO}_2$  and  $\text{Ni}/\text{CeZrLa}$  respectively. The preexponential factor was pressure dependent, showing a decrease with the increase of the operating pressure, especially in the  $\text{Ni-Pt}/\text{CeO}_2$  case. Kechagiopoulos et al. studied the kinetics of low temperature steam reforming of methane over nickel and rhodium catalysts that were supported on lanthanum-doped ceria-zirconia oxides, in combination with hydrogen selective membranes [57]. The temperature programmed steam-reforming experiments and isotopic investigations, by using  $\text{CD}_4$ , revealed that the C-H bond activation is the kinetically controlled step, for both the metals; moreover, the rate was not affected by steam. The microkinetic model was developed with a FORTRAN-based (micro) kinetics-modeling platform, to study the conversion surface pathways and the reactants activation. The simulation and experimental results matched to identify the dehydrogenation of the methyl surface species as the rate-determining step for both the metals, and the higher activity of rhodium. Mundhwa et al. studied the kinetics data of methane steam reforming, while using the Ni-spinel catalyst that was supported on alumina and yttria-stabilized-zirconia [58]. The experiments were carried out with a steam to carbon ratio of 1.25 and 1.50, at isothermal plug-flow conditions, at atmospheric pressure, and at five different contact times, between 55 and 277 ms, at three different temperatures: 700 °C, 800 °C, and 900 °C. The simulation was made in a one-dimensional (1D) plug flow reactor model, while using the COMSOL<sup>TM</sup> environment, while the surface microkinetic model was adopted from the literature and validated by optimizing the kinetic parameters. The most influential elementary reaction steps were selected with a stepwise approach based on the partial equilibrium analysis and the local sensitivity analysis. A MATLAB programming code for transient series-CSTR model was developed to minimize the objective function. The optimization showed that  $\text{CH}_4(\text{s})$  dehydrogenation of surface,  $\text{CH}(\text{s})$  or  $\text{CH}_2(\text{s})$  formation and the consumption of surface,  $\text{H}_2\text{O}$  adsorption,  $\text{H}(\text{s})$  desorption,  $\text{CO}(\text{s})$  formation are the most influential steps, in the selected operating conditions. The introduction of yttria into  $\text{ZrO}_2$  structure, increase the activity of the oxygen ( $\text{O}_2$ - or  $\text{O}$ -) pumping component. German et Sheintuch studied the methane steam reforming kinetics, at 600 °C on platinum (111), rhodium (111), and nickel (111) surfaces, by numerical simulation of the microkinetic models, while using the rate constants that were calculated in previous works [59]. The individual rate constants are classified in three categories, as follows:  $\text{CH}_4$ ,  $\text{H}_2\text{O}$ ,  $\text{CO}$ , and  $\text{H}_2$  adsorption and desorption and C–O bond dissociation and formation, which were calculated using transition state theory, A–H bonds ( $A = \text{C}, \text{O}, \text{and H}$ ) dissociation and formation, which were calculated from the

thermal metal lattice vibrations and H tunneling through a potential barrier, depending on the distance of AH from a surface. The studies on platinum surface revealed a linear dependence between the rate and methane pressure, while, in the case of the nickel surface, the linear dependence occurred up to 2-bar methane pressure at a water pressure of 0.25-bar. The rate on rhodium surface showed a maximum at a methane pressure  $\approx 0.75$ -bar, due to blocking of all active sites by adsorbed CH species. Thallam Thattai et al. reported an experimental study on methane steam reforming global kinetics, for single operating SOFCs with Ni/gadolinium doped ceria anodes, at a low steam to carbon ratio and moderate current densities [60]. Power law and Langmuir–Hishelwood rate expressions were compared and the limitation in using them for complete cermet anodes were identified. The two models predicted the same methane steam reforming reaction rate, however a significant difference in the local rate and species distribution was found. The Langmuir–Hishelwood approach predicted a much higher reaction rate near the anode inlet; however, both the models showed a large dependency of the reaction orders and exponents on the local current density, and that the electrochemical oxidation promotes methane conversion and the reaction rate. No carbon deposition was observed with a steam to carbon ratio 1.0–1.5. Che et al. studied the deactivation, due to coke formation, of nickel-based catalysts for methane steam reforming reaction, by combining density functional theory calculations and experimental works [61]. The microkinetic model was developed in the presence and absence of electric fields, demonstrating that the presence of electric fields gives rise to changes in the reaction mechanism, to the decrease of the surface coverage of carbon, to the increase of the water coverage, to the acceleration of the rate-limiting step of the C-H bond cleavage and the increase of the desorption rates of the produced syngas. The results of this study demonstrated that a positive electric field allows for reducing the steam to methane ratio and operating temperature, when compared to the case in which the electric field is not present; moreover, the nickel-based catalyst retains the high catalytic activity, even at industrially relevant pressures. Khzouz et al. studied the Ni/Al<sub>2</sub>O<sub>3</sub> catalytic system, experimentally and numerically by means of COMSOL Multiphysics®5.0, for low temperature methane steam reforming [62]. The activity tests were carried out in the temperature range of 500–700 °C and at a steam to carbon ratio of 2 and 3, under atmospheric pressure. The experimental results were used to validate the simulation data, which were based on the yields of H<sub>2</sub>, CO<sub>2</sub>, and CO. The maximum hydrogen yield was achieved at 700 °C, however the thermogravimetric analysis tests highlighted the catalyst to be prone to deactivation (Figure 1).

Ji et al. developed a fluid dynamic model to study the methane steam reforming process in a sorption enhanced palladium-based membrane reactor, while using a Ni-based catalyst and Na<sub>2</sub>ZrO<sub>3</sub> as CO<sub>2</sub> sorbent [63]. The comparison between a traditional membrane reactor and sorption enhanced membrane reactor showed that the last provides an increase in the reaction rate, i.e. methane conversion and hydrogen yield, and a decrease of the CO<sub>2</sub> fraction. The CO fraction decreased by one order of magnitude; moreover, the poisoning effect of carbon monoxide on the membrane can be minimized by the CO<sub>2</sub> capture. de Oliveira Rocha et al. studied the effect of addition of Au to 15% Ni/Al<sub>2</sub>O<sub>3</sub> catalysts in steam reforming of methane [64]. DRIFTS-CO showed that gold modified the surface structure of nickel, by blocking the low coordination Ni sites with high electron density and high activity in CH<sub>4</sub> activation, and changing the type of CO adsorption, from bridge to linear form. The increase of the apparent energy activation was related to the blocking of the Ni sites, as the results of the decrease in the overall electron density, which disfavor the CH<sub>4</sub> activation and decrease the stability of the carbon intermediates.

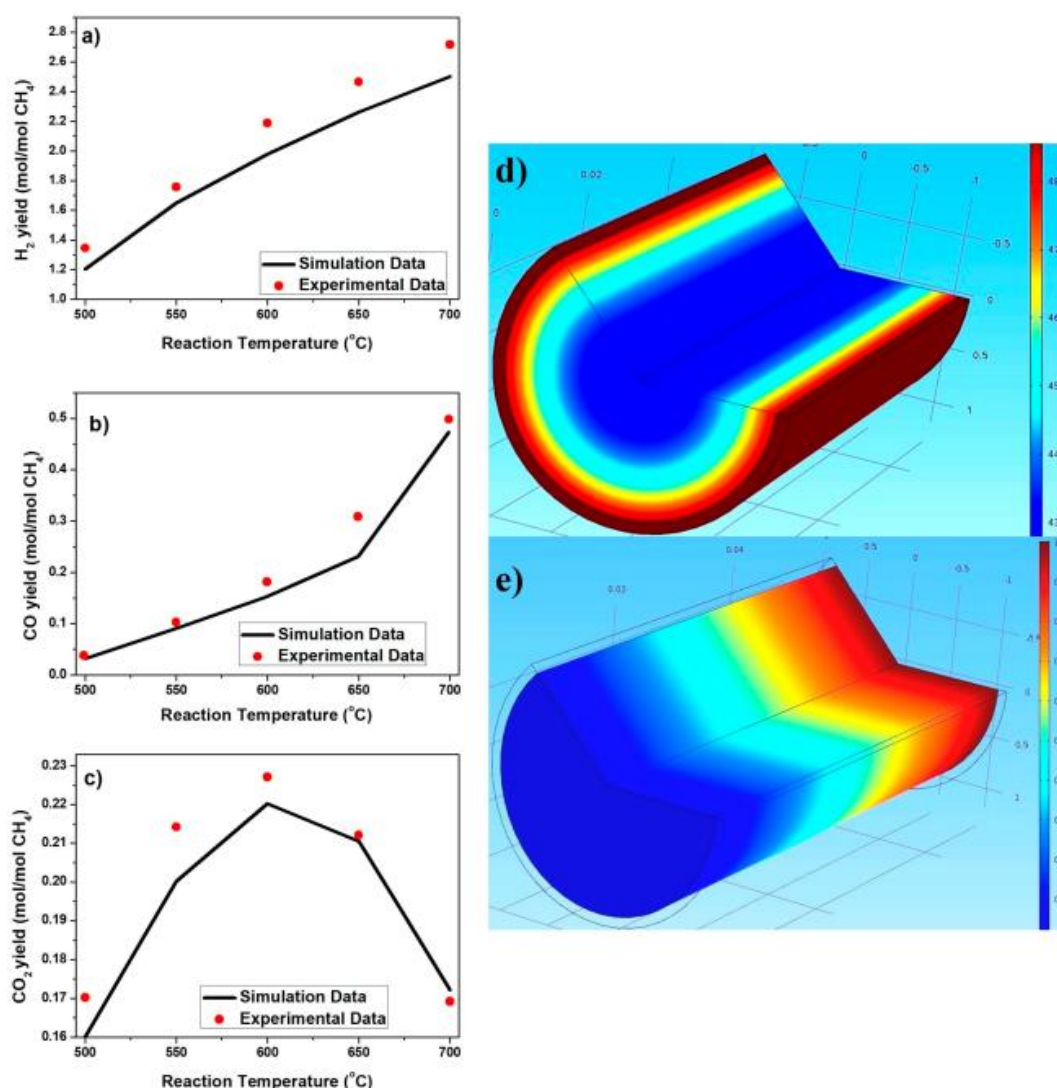


**Figure 1.** Validation of experimental results with the simulation data for 10% Ni/Al<sub>2</sub>O<sub>3</sub> catalyst within 500–700 °C and S/C of 2 under atmospheric pressure; (a) H<sub>2</sub> yield, (b) CO yield, (c) CO<sub>2</sub> yield, (d) Catalyst bed temperature distribution, and (e) H<sub>2</sub> pressure distribution [62].

Pashchenko studied the methane steam reforming with a mixture of methane combustion products, by coupling experimental and theoretical studies, on commercial Ni-based catalysts [65]. The chemical composition of the catalyst was: 14.5% of NiO, 0.2% of SiO<sub>2</sub> with respect to the support, whose composition was CaO-MgO-La<sub>2</sub>O<sub>3</sub>-Al<sub>2</sub>O<sub>3</sub>. The experimental procedure was performed by varying some operational parameters, such as the temperature in the range 400–800 °C, the residence time, the pressure from 1 to 5-bar, and the composition of the inlet reaction mixture (steam to CH<sub>4</sub> ratio = 0–2). The thermodynamic analysis was performed by means of Aspen-HYSYS version 8.4, the total Gibbs free energy minimization was used to determine the maximum methane conversion achievable. The methane conversion approached the equilibrium at the residence time of above 4.0 kgcat\*s/mol. The methane conversion was almost proportional to the residence time for temperatures below 700 °C, while, above 800 °C, the methane conversion at a low residence time increased faster than for a high contact time. The effect of pressure (in the pressure range from 1- to 5-bar) on methane conversion was negligible. For the stoichiometric methane to steam ratio, the conversion decreased with the temperature, with the increasing of time on stream. In another study, Pashchenko presented a computational fluid dynamics model of the methane steam reforming over pre-heated Ni-based catalyst, developed via ANSYS Fluent, for real computational domain of the reformer [66]. The results

showed that each 100 mm of catalyst bed, the pressure drop was about 160 Pa, no significant gradient was present along the radial axis of the reformer, at the catalyst temperature of 1300 K the syngas composition approached to equilibrium. The highest temperature gradient was observed at the section near the reformer inlet, where the highest reaction rate and the highest temperature drop between the catalyst and the reactor flow was observed. Unruean et al. developed a kinetic Monte-Carlo model to simulate the methane steam reforming on Ni/MgAl<sub>2</sub>O<sub>4</sub> catalyst [67]. The simulation showed that the reaction took place at both the low mole fraction of methane ( $y_{\text{CH}_4} = 0.1$ ) and at the high mole fraction of methane ( $y_{\text{CH}_4} = 0.9$ ), as the result of the high coverages of H\* and O\* at low  $y_{\text{CH}_4}$ , and the high coverage of C\* and CH<sub>3</sub>\* at high  $y_{\text{CH}_4}$ , respectively. The highest hydrogen production rate was in the mole fraction 0.4–0.5 of methane, where the oxidation of CH<sub>x</sub>\* intermediates became the crucial reactions. Moreover, the hydrogen production rate increased with the pressure until 10-bar, but, above, it dropped remarkably (Figure 2).

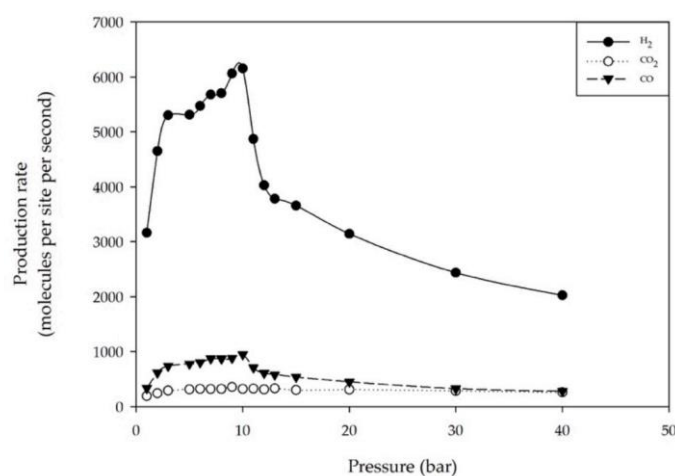


**Figure 2.** Production rate as function of the total pressure,  $T = 550\text{ }^{\circ}\text{C}$  and  $y_{\text{CH}_4} = 0.5$  [67].

Liu et al. reported a density functional study on the use of Ni/CaO based bifunctional catalyst in the sorption enhanced methane steam reforming, with a focus on the coke resistance [68]. The results showed that calcium could enhance the mobility of the oxygen atoms on the surface, thus improving the elimination of the carbon atoms through the oxidation to carbon monoxide. Moreover, the presence of calcium facilitated the water dissociation to produce enough oxygen intermediates for carbon oxidation. Calcium slowed down the carbon diffusion and the C–C formation rate, thus inhibiting the carbon deposition. Vogt et al. studied the effect of the SiO<sub>2</sub>-supported nickel nanoparticle size, in the range 1.2–6.0 nm, on the methane steam reforming and dry methane reforming, by operando infrared spectroscopy, to determine the active mechanism and its kinetic dependence on the nickel particle size [69]. The results showed that very small supported Ni nanoparticles (<1.5 nm) were less active in the reforming processes, probably due to the quantum effects, which may play a rule for small nanoclusters. There was a dependence between the particle size and TOF, with a maximum for 2–3 nm particle size; moreover, an increasing of the carbon formation was observed in methane steam reforming for larger nanoparticle sizes. The predominant pathway for syngas formation was the direct carbide pathway, the rate determining step was dependent on the ratio of the feedstock that was applied to the system and the activation of methane; moreover, the recombination of C and O to form CO and the desorption thereof were also limiting factors. Chen et al. reported an experimental and numerical study on the intrinsic kinetics of methane steam reforming, while using a micro fluidized bed, with a 50wt/NiO/ $\alpha$ -Al<sub>2</sub>O<sub>3</sub> catalyst [70]. FLUENT was the software used for the simulation, while the model was used to simulate the effects of the steam-to-carbon ratio, the inlet velocity, and the preheating temperature. The activation energies for CO and CO<sub>2</sub> formation resulted in 81.69 kJ/mol and 59.38 kJ/mol, respectively, while the pre-exponential factors were 316.6 mol/ghkPa<sup>0.85</sup> and 0.00263

mol/ghkPa<sup>3.1</sup>, respectively. The rate of CO formation increased with the reaction temperature, while the CO<sub>2</sub> formation decreased with the reaction temperature. At 800 °C, the methane conversion is 92.28%, the hydrogen production is 3.34, and the selectivity to CO 0.99. The CH<sub>4</sub> conversion, the hydrogen yield, and CO selectivity increased with the steam to carbon ratio; at 700 °C, when the inlet velocity is 0.2 m/s (residence time of 0.5 s), the CH<sub>4</sub> conversion is over 95%.

### 3. Ni Based Structured Catalysts

The aim of a distributed hydrogen production, for example, through an on-site type hydrogen station, is only reachable if a novel reforming system is developed, with some unique properties that are not present in the large-scale reforming system. These properties include, among the others, (i) daily startup and shutdown (DSS) operation ability, (ii) rapid response to load fluctuation, (iii) compactness of device, and (iv) excellent thermal exchange. In this sense, the catalyst has an important role. The fixed-bed reaction system that is adopted in the large-scale hydrogen manufacturing process cannot satisfy such properties, even if, in the last years, several studies were performed to optimize the catalyst shape, so minimizing the pressure drop and increasing methane conversion. In literature, different papers in which researchers performed experimental and simulation investigations on the role and effect of the Ni-based catalyst shape in packed bed reactors for MSR are present. In the paper of Buwa et al. [71] the authors analyzed, through particle-resolved CFD simulations of multilayered packed beds, the effect of different boundary conditions and particle modeling approaches. In particular, the simulations had the aim of understanding the effect of particle shape on pressure drop ( $\Delta P$ ), dispersion, methane conversion, and effectiveness factors for methane steam reforming reactions. With this aim, 30 Ni- $\alpha$ Al<sub>2</sub>O<sub>3</sub> particles with different shapes (trilobe, daisy, hollow cylinder, cylcut, and seven-hole cylinder), as shown in Figure 3, with a tube to particle diameter ratio of 5, were considered. The authors developed a modified correlation that was able to predict  $\Delta P$  for the particles with different shapes, since the empirical correlations usually used (Ergun and Zhavoronkov et al.) over-predicted the  $\Delta P$ . The results showed that the catalyst shape has an important effect: lower  $\Delta P$  and higher dispersion can be obtained while using the externally shaped particles (trilobe and daisy), since they are characterized by a lower surface area and higher back flow regions, while higher CH<sub>4</sub> conversion and effectiveness factors can be obtained while using the internally shaped particles (cylcut, hollow, and seven-hole cylinder), since they assure the better access for the reactants. Among all, the cylcut-shape allowed for obtaining the best compromise between CH<sub>4</sub> conversion and  $\Delta P$ .

Pashchenko investigated the effect of the Ni- $\alpha$ Al<sub>2</sub>O<sub>3</sub> catalyst shape on the methane conversion and pressure loss in a packed bed reactor for MSR in a recent paper [72]. The author performed different experimental tests at a constant packed bed length (600 mm), in particular by varying the shape (a simple cylinder, a Raschig ring, a seven-holes cylinder, and a seven-holes sphere), and, in the case of the simple cylinders and the Raschig rings, also the end-to end dimensions (5 mm, 10 mm, 15 mm, 20 mm, and 25 mm) were varied. The results showed that, as expected, the catalysts shape is important for determining the methane conversion and pressure drop. In particular, the seven-holes spheres allowed obtaining the maximum methane conversion and the minimum pressure drop, due to their higher surface area. Furthermore, it is reasonable thinking that the improvement of the performance of the steam methane reforming reactor can be obtained by increasing the geometric surface of the packed bed since the catalytic activity of the surface unit of all investigated catalysts was not dependent from their shape. Also the reduction of the size of the catalyst particles allowed for increasing the methane conversion at a constant weight residence time [72].

Park et al. also faced the problem of the intensification of MSR fixed bed reactors [73], with the aim to identify and solve the typical problems occurring in the scale up of the process. So, the authors performed several experimental tests by using lab- and bench-scale reactors, investigating the effects of different reaction parameters, such as temperature, pressure, steam/methane ratio, and space velocity, on hydrogen production. The lab-scale tests allowed for the design of the bench-scale reactor, which is characterized by three consecutive heaters, and in which the thermodynamic and kinetic data that

were obtained using the lab-scale reactor were used for choosing the operating conditions. The results showed that a methane conversion higher than 90% and a hydrogen production higher than 10 L/min. was obtained in the bench-scale reactor only if all three consecutive heaters were able to heat the system up to 800 °C, at the gas-hourly space velocity of 2.0 L CH<sub>4</sub>/(h·g<sub>cat</sub>). Furthermore, the author proposed an effective shutdown and startup procedure, which was able to prevent catalyst deactivation during the shutdown, as well as allowed for decreasing the time and costs that are involved in the startup.

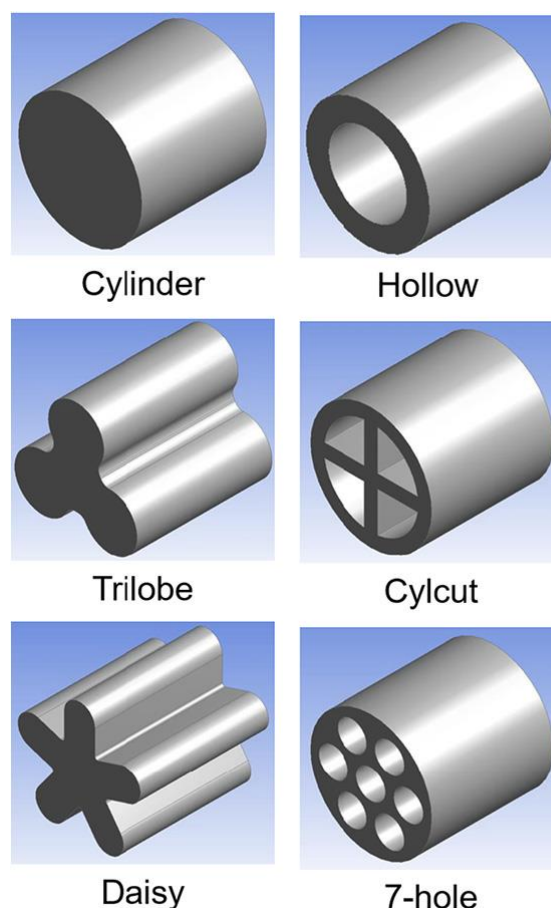


**Figure 3.** Packing shapes considered in the work of Buwa et al. [71].

Ko et al. [74] investigated the performance in MSR reaction of two Nickel-based catalysts, which were prepared using cylinder-shaped alumina pellets as supports: (i) egg-shell-type catalysts, in which nickel was selectively located in the outer region of the alumina pellets, by means of ethylene glycol or 1-octanol as hydrophobic solvents (in order to avoid or retard the internal penetration of the alumina pellets by the nickel nitrate solution), and (ii) ‘homo-type’ catalyst, with even nickel distribution inside the alumina pellets. The results highlighted that, in the case of the homo-type catalyst, the Ni loading has a fundamental role, since a loading of 3.5 wt % did not allow for obtaining high methane conversion, while a loading of 10 wt % assured the same methane conversion of a commercial catalyst used as reference. On the other hand, egg-shell-type catalyst with a nickel loading of 3.5 wt % showed almost the same methane conversion as those of 10 wt % ‘homo-type’ catalyst and the reference catalyst, so indicating that egg-shell-type catalysts were potentially feasible for use as MSR catalysts.

Apart from the intensification of MSR fixed bed reactor, in the way of an innovative distributed hydrogen production, the adoption of a different concept from the fixed-bed reaction system is necessary for the development of a novel reforming system. This concept includes the use of microstructured catalytic reactors or the use of structured catalytic reactors. In particular, the latter are very promising,

since it is possible the integration and the optimization of the chemical (catalytic activity and selectivity) and the physical (enhancement of heat-transfer, rectifying property of flow, and lower pressure drop) properties by depositing a catalytic component onto a metallic or ceramic substrate with high thermal conductivity, thus resulting in an effective process intensification [75].

### 3.1. Microstructured Catalytic Reactors

Some advantages that are characteristic of microreactors, such as (i) the reduced dimensions, included the weight, and compact design, (ii) the improved heat- and mass-transfer efficiencies, (iii) enhanced lifetime of catalyst, and (iv) higher conversion, yield, and the selectivity that they allow obtaining, made these reactors increasing the attention of the scientific community. The typical microreactor is designed to provide inside it mostly a laminar ( $1 < Re < 1000$ ), directed, and highly symmetric hydrodynamic flow and decreased interparticle mass-transfer resistance. In this way, a better and faster contact between reactants and catalyst, as well as more uniform temperature and concentration profiles, are assured due to the high surface to volume ratio. In addition, the possibility to realize in the microreactors the precise control of the main features, temperature, pressure, residence time, and flow rate, allowed for performing explosive and highly exothermic reactions with less risks than conventional processes [76]. All these positive features make possible an effective increase of the MSR process efficiency by using the micro-channel reactors, so favoring the increase of space time yields to approach the industrial requirement. Various micro-reactor types, such as coated wall micro-reactors, packed-bed micro-reactors, structured catalyst micro-reactors, and membrane micro-reactors, have been tested and used for hydrogen production [77].

Regarding the hydrogen production by means of MSR in microreactors, Chadwick et al. [76], developed a micro-structured catalytic hollow fiber with low mass- and heat-transfer resistance, by incorporating Ni/SBA-15 catalyst into alumina hollow fibers. The 5–25  $\mu\text{m}$  widely opened radial microchannels that were present on the inner surface of the hollow fibers were responsible of the good catalyst incorporation and contributed to higher interaction between the reactants and catalyst, resulting in a higher catalytic performance. The authors compared the methane conversion that was achieved from both ceramic hollow fiber (CHF) reactor and the classical packed bed reactor, and the results showed that, in both cases, a methane conversion close to thermodynamic equilibrium values (around 25% at 465 °C) was reached. However, in the case of the CHF configuration containing Ni/SBA-15 catalyst, a space velocity approximately 6.5 times higher was used. More important, the CHF configuration allowed for obtaining a higher  $\text{CO}_2$  selectivity and an increased productivity rate, and this last result confirmed their potential for further reducing the required catalyst.

Cheng et al. [77] studied the effect of temperature, steam-to methane ratio, GHSV at high pressure varied from 0.5 MPa to 2.0 MPa on the catalytic performance of Ni catalyst plate for methane steam reforming reaction in micro-channel reactors. The results showed that, at  $240,000 \text{ h}^{-1}$ , the methane conversion approached the thermodynamic equilibrium value at 900 °C and 2.0 MPa, hence indicating that micro-channel reactor with coated catalyst is feasible and highly efficient for MSR process. In these conditions, the authors reported a hydrogen productivity of about  $0.1 \text{ m}^3/\text{h}$  in a single channel at 2.0 MPa, which corresponded to  $1.95 \times 10^4 \text{ m}^3/(\text{m}^3 \text{ h})$  space time productivity.

Kincal et al. [78] studied the possibility of performing the steam methane reforming reaction over Ni/mullite and Pd/CeO<sub>2</sub>/mullite catalysts by using the solar energy as power source. In particular, a parabolic mirror with a 70 cm was used; so, delivering concentrated solar flux onto a focal area of about 3 cm in diameter. The authors compared the performance of powder and microstructured reactors monolith (mullite) catalysts. The results evidenced a CH<sub>4</sub> conversion that was higher than 90% for both the samples, but a coke deposition was observed over the 15% Ni/Mullite monolith. These results, even if very interesting due to the renewable power source used, denoted the need for further improvements. In fact, the coke formation must be decreased, in order to increase the lifetime of the catalyst. For example, more consistent water vapor delivery can be performed, or the catalyst formulation can be optimized.

### 3.2. Structured Catalytic Reactors

As it is well known, the industrial steam reforming plant is composed by more than 100 tubular reactors with a length of 10–14 m, which are placed in a large furnace, in which the gas burners are positioned for an optimal distribution of heat among the reactor tubes. The temperature outside the tubular reactors must be considerably higher than 1000 °C, in order to generate the necessary inward heat flux, as illustrated by the temperature profile in Figure 4 [79].

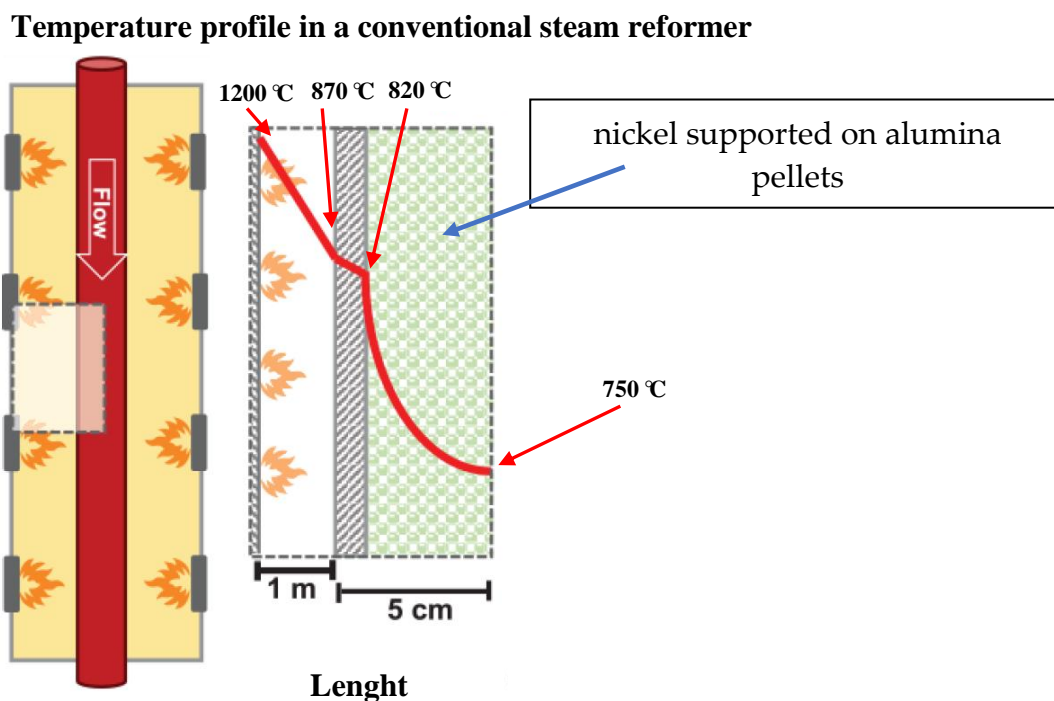


**Figure 4.** Temperature profile in a conventional steam reformer.

The most used catalysts used in the commercial MSR process are doped nickel based catalysts that are supported on alumina pellets (Ni/M-alumina, M = Mg, Ca etc.) or on magnesium aluminate (Ni/MgAl<sub>2</sub>O<sub>4</sub>), with the reaction temperature around 700–800 °C (Figure 4).

As a critical issue, in the MSR reforming process, the limiting step is the heat transfer towards the reaction volume, since its high endothermicity requires high heat fluxes, and the catalyst has low thermal conductivity: so the thermal profile showed in Figure 4 occurs [80]. Such a constraint imposes complex reactor geometries and very high temperatures of heating medium, thus resulting in very expensive construction materials, very high reaction volumes, and very slow thermal transients. Therefore, it causes an increase of the operative and fixed costs and a reduction of the overall process efficiency.

A flatter axial thermal profile through the catalytic bed can be achieved by using high thermal conductivity carriers (such as monoliths or foams), leading to heat redistribution along the catalytic bed, with a consequent higher hydrocarbon conversion. In addition, the highly conductive supports ensure a more uniform radial temperature profile, thus resulting in better heat transfer and a reduction of hot-spot phenomena and very stable performances.

In the perspective of process intensification, dedicated studies have demonstrated that the use of a carrier with a high thermal conductivity can allow for obtaining better catalytic performance. The main studied carriers can be divided in two groups: (i) metallic and (ii) ceramic, as reviewed below.

#### 3.2.1. Metallic Carriers

The most investigated metallic carriers are the honeycomb fin (Figure 5), on which the active species are deposited by means of different techniques.



**Figure 5.** Stainless honeycomb monolith [81].

Fukuhara et al. studied the effect of the preparation procedure on the reforming performance of a nickel-based metal honeycomb-type catalyst in 2015 [75]. The authors prepared the catalyst while using the combined technique of the sol-gel method and the electroless plating on the stainless-steel substrate, by varying (i) the reducing agents in the plating bath ( $\text{NaH}_2\text{PO}_2$ ,  $\text{NaBH}_4$ , or  $(\text{CH}_3)_3\text{NBH}_3$ ), (ii) the plating time, and (iii) the nickel source ( $\text{NiCl}_2$ ,  $\text{NiSO}_4$ , or  $\text{Ni}(\text{NO}_3)_2$ ). The results showed that the honeycomb catalyst that was prepared by using  $\text{NaBH}_4$  with a plating time of 3 min. and chloride or sulphate as nickel source, demonstrated a higher methane steam reforming performance than the commercial catalyst. The authors also studied the effect of the addition of a promoter component to the aluminum sol solution, by adding Ce, Y, Mg, or Zr, and the reforming property of the catalyst that adds the Ce component was improved.

Xu et al. investigated the effect of the pretreatment on the performance of catalytic  $\text{Ni}_3\text{Al}$  foils for steam reforming of methane [82]. The authors set up a pretreatment procedure that consists of water vapor oxidation followed by  $\text{H}_2$  reduction, and the results indicated that the catalytic activity and selectivity of the  $\text{Ni}_3\text{Al}$  foils towards MSR was enhanced when a water vapor treatment at 600–700 °C, followed by  $\text{H}_2$  reduction at 600 °C, occurred. The authors highlighted the formation of a multi-layer surface structure on the foils after pretreatment, consisting in fine Ni particles on the outermost layer, with subsurface layers consisting of  $\text{NiAl}_2\text{O}_4$  and  $\text{Al}_2\text{O}_3$ , which, in their opinion, was responsible of the enhancement of catalytic properties.

Mundhwa et al. investigated the influence on MSR of different configurations of the coated combustion-catalyst (platinum-alumina) in a catalytic plate reactor (CPR), by means of simulation models. In one research, they compared a segmented configuration (SLCC-model) with a continuous configuration (CLCC-model) [83]. In a following research, they extended their studies, by simulating four different computational models with four different combinations of segmented and continuous configurations, (i) Continuous Combustion-catalyst and Continuous Reforming catalyst (CCCR), (ii) Continuous Combustion-catalyst and Segmented Reforming catalyst (CCSR), (iii) segmented combustion-catalyst and continuous Reforming catalyst (SCCR), and (iv) segmented combustion-catalyst and segmented reforming catalyst (SCSR), between the combustion-catalyst and reforming-catalyst [84]. In both researches, the authors investigated the influence of flow direction, gas hourly space velocity (GHSV), and reforming-catalyst thickness on the performance of CPR. The results showed that the best performance in terms of methane conversion and hydrogen production, as well as in terms of minimizing the maximum reactor plate temperature, axial thermal-gradients, and thermal hot-spots, were obtained by using the segmented combustion-catalyst in co-flow mode. In fact, this configuration assures a continuous supply of heat to the reforming-side from the combustion-side through the interspacing among active combustion-catalyst segments. In this way, the formation of cold and hot zones is avoided and a balanced thermal distribution at the reactor downstream is

obtained. In addition, the authors showed that the CPR that was designed with SLCC configuration required both less combustion feed flow (about 7 to 8%) and combustion-catalyst (about 70% less) to produce the required hydrogen flow (29.80 mol/h) to feed a 1 kW fuel cell as compared to the CPR designed with CLCC. Moreover, a significant reduction and the complete disappearance of the thermal hot spots at the initial length of the catalysts are observed with the SCSR and SCCR configurations, respectively, when compared to the conventional CCCR design. In addition, the authors reported that both reforming-side and combustion-side effective thermal conductivities were noticeably improved for the first 44% and 36% of the catalyst length in a CPR that was designed with the SCSR and SCCR configurations, respectively, when compared to the CCCR configuration.

Tightly rolled Ni coil catalysts were extensively studied by the research group of Hirano, Xu et al. The authors assembled and tested in MSR a tightly rolled Ni coil catalyst using only 30 mm-thick pure Ni foils, in a wide range of space velocities (455–2800 h<sup>-1</sup>) and S/C (0.62–2.48) ratios [85]. The results showed that the high geometric surface area per catalyst volume (88.1 cm<sup>2</sup>/cm<sup>3</sup>) that was achieved for the Ni coil catalyst allowed for obtaining a high H<sub>2</sub> production rate per unit catalyst volume and a high CH<sub>4</sub> conversion, so demonstrating the high potential of this kind of catalyst for small-scale hydrogen production systems. The authors continued their researches by assembling and testing, in MSR, a tightly rolled Ni coil catalyst, always using only 30 mm-thick pure Ni foils, with a higher cpsi (about 2300) if compared to the previous one (about 700) [86]. The results showed that the honeycomb catalyst with higher cpsi showed higher catalytic activity for methane steam reforming at low S/C (1.36) and high GHSV (6400 h<sup>-1</sup>) than the one with lower cpsi. The authors also performed isothermal tests at 800 °C, and the results showed a decrease in the catalytic activity of the honeycomb catalyst in first hours, up to reaching the stable value of about 40%. In-situ XAFS measurements revealed that the decrease in activity at temperatures lower than 750 °C was due to the oxidation of surface Ni atoms during the catalytic reaction. Subsequently, the authors investigated the influence of steam treatment and hydrogen reduction on the catalytic activity of the pure Ni honeycomb catalyst with the higher cpsi [87]. The results showed that a steam treatment and subsequent hydrogen reduction at a temperature higher than 800 °C enhanced the catalytic activity of the Ni honeycomb catalyst. The authors attributed this enhancement to the combined effect of the two treatments: in fact, the steam treatment is responsible for the formation of fine Ni oxide particles, which are reduced to metallic Ni on the surface during the hydrogen reduction, hence suggesting a structure sensitivity of the MSR.

Settar et al. compared four different Wall-Coated Steam Methane Reformer (WC-SMR) with a catalytic surface [88]. In particular, the authors compared a classical WCSMR, with three modified configurations, in which three different inert Metal Foam (MF) matrices were inserted in the catalytic region: Ni-Foam, Ni-Cr-Foam, and Ni-Fe-Cr-Foam, identified as MF (A), MF (B) and MF(C), respectively.

The results showed that the use of MF in such configurations increased the CH<sub>4</sub> conversion, since they allowed for a good heat distribution inside the system and better contact among the gas mixture and the catalyst particles, as well, as they were able to reduce the gas mixture velocity. In particular, the inert Ni-Fe-Cr-Foam, MF (C) resulted in the most significant improvement of the conversion rate, 18.64%, and of H<sub>2</sub> production, 16.91%, when comparing to the clear WC-SMR. These results confirmed the possibility to enhance the MSR by adding inert metallic foam in the catalytic region of a WC-SMR; one possible optimization of this system could be the use of catalysed metallic foams.

Ashraf et al. investigated the preparation, characterization, and testing in MSR of FeCrAlloy@monoliths with different cell density (461–1367 cpsi), catalysed with different loadings of Ru/La-Al<sub>2</sub>O<sub>3</sub> (100–200 mg) [89]. The results showed that the methane conversion increased with increasing temperature, catalyst loading, and cell density. In particular, in correspondence of the same washcoat thickness (about 20.6 μm), the higher cell density monolith showed 13.6% higher methane conversion at 600 °C, weight hourly space velocity (WHSV) = 55 NL h<sup>-1</sup> g<sub>cat</sub><sup>-1</sup>, and ratio S/C = 3.0, as compared to the lower cell density one.

Shigarov et al. investigated the performance of a compact (800 cm<sup>3</sup>) membrane reformer module to produce 0.25–0.30 Nm<sup>3</sup>/h of hydrogen by MSR by means of experimental tests and modelling [90].

The module consists of a two-sided composite membrane disc with a 50 mm Pd-Ag layer and two adjacent 4 mm thick Ni foam discs (60 ppi). A nickel catalyst and porous support were deposited on the foam discs to give the final composition of 10%Ni/10%MgO/Ni-foam. The modules were tested at a 8–13-bar pressure of the mixture in the reforming zone and at 1-bar of pure hydrogen under the membrane,  $H_2O/C = 2.5\text{--}3$ , and a module temperature of 550–680 °C (with and without hydrogen removal). Calculations were made for revealing the effect of thickness of the Pd-Ag membrane layer (5–50  $\mu\text{m}$ ), thickness of the Ni foam discs (0.5–8 mm), and temperature (600–700 °C) on the hydrogen output of the module in order to optimize construction of the module. The results evidenced a production of hydrogen higher than 0.7 kg( $H_2$ )/h/m<sup>2</sup> and an energy production higher than 1 MW/m<sup>3</sup>.

Payak et al. proposed an innovative Methane Steam reforming reactor, whose novelty consisted in dividing it into segments of various lengths and reactivity. In particular, the catalyst (nickel and yttria-stabilized zirconia) was splitted and the created empty volume was filled with porous, nonreactive, thermal conducting metallic foam [91]. This approach allows for moderating a sharp temperature drop at the inlet of the reactor typical for the endothermic methane/steam reforming process. The authors developed and implemented an in-house solver for the mathematical and numerical models of transport phenomena and the reaction kinetics (taken from the literature). The results of the model were compared with the experimental tests, which were performed by varying the number and lengths of catalytic and non-catalytic segments, and good agreement was found. The results indicated that a reduction of the difference between the maximum and minimum values of the temperature inside the reactor occurred, and the conversion rate decreased 15% in correspondence of a reduction of catalyst of a half, so evidencing that it is possible to realize a reactor for steam reforming, with less catalyst used and obtaining the same methane conversion rate as the reference case with relatively small elongation of reforming unit.

Deo et al. investigated the effect of adding Rh to 15 wt % Ni/MgAl<sub>2</sub>O<sub>4</sub> catalyst for the MSR [92]. In particular, the authors washcoated FeCrAlloy metal monoliths with a 0.5 wt %Rh-15wt %Ni/MgAl<sub>2</sub>O<sub>4</sub> catalyst and compared its performance with a packed bed and a 15%wtNi/MgAl<sub>2</sub>O<sub>4</sub> washcoated metal monolith. The results evidenced that, in the operating conditions of  $T_{\text{wall}} = 600\text{ °C}$ ,  $P = 1\text{-bar}$ , ratio  $S/C = 5$ ,  $GHSV = 6000\text{ h}^{-1}$ , and  $W/F_{\text{ao}} = 0.34\text{ g}_{\text{cat}}\text{-h/gmol}$ , the Rh-Ni/MgAl<sub>2</sub>O<sub>4</sub> washcoated metal monolith showed the best performance in terms of methane conversion (about 50%) if compared to NiMgAl<sub>2</sub>O<sub>4</sub> washcoated metal monolith and packed bed reactor (about 40% and 25%, respectively).

Recently, Tronconi et al. proposed and tested in MSR an innovative fixed bed reactor configuration, consisting in small catalytic pellets filling the voids of highly conductive metallic open-cell foams [93]. The aim was to enhance the radial heat transfer of the tubular reactor by using a high thermal conductivity solid. In particular, alumina egg-shell particles with diameter of 600  $\mu\text{m}$ , catalysed with Rh/Al<sub>2</sub>O<sub>3</sub>, were used to fill the voids of FeCrAlY open cell foams of 12 PPI and copper open cell foams of 10 and 40 PPI. The results of the tests, which were performed at GHSV of 5000 and 10,000 h<sup>-1</sup> in the temperature range 600–800 °C, highlighted the benefits in terms of thermal management of the reactor and an increase of productivity at the same furnace temperature in kinetically-limited conditions. The authors, based on the electric equivalent circuit approach, also developed a heat transfer model of the packed foams, incorporating independently estimated lumped or effective parameters, thus providing an engineering rationale of the observed reduction of temperature gradients across the catalytic bed.

Table 3 summarizes the main performances of the packed bed reactors and of the catalysts supported on metallic carriers.

**Table 3.** Summary of the main performance of the packed bed reactors and of the catalysts supported on metallic carries, compared with a micro-channel catalytic reactor.

Structured Carrier Shape	Catalyst	Operating Conditions	Main Characteristics	Main Performance	Ref.					
Ceramic Packed bed			Surface area, mm <sup>2</sup>	DP, Pa	T <sub>s</sub> , °C *	Q <sub>sink</sub> , W *	X <sub>CH<sub>4</sub></sub> , % *	η <sub>1</sub> *	η <sub>3</sub> *	
Cylinder	Ni/αAl <sub>2</sub> O <sub>3</sub>	Initial mass fractions CH <sub>4</sub> = 0.1966 H <sub>2</sub> = 0.0005 CO = 0.0007 CO <sub>2</sub> = 0.1753 H <sub>2</sub> O = 0.6269 Re <sub>t</sub> = 50,000	1885	1109	723.87	1159	1.984	0.269	0.452	[71]
Trilobe			1637	165	727.96	787	1.373	0.393	0.595	
Daisy			1955	164	732.33	868	1.475	0.438	0.639	
Hollow			2428	197	742.47	1062	1.831	0.551	0.766	
Cylcut			3484	208	750.66	1243	2.136	0.689	0.857	
7-hole			3737	218	752.06	1283	2.187	0.690	0.865	
Cylinder	NiO = 14.5%; SiO <sub>2</sub> = 0.2%; support CaO-MgO- La <sub>2</sub> O <sub>3</sub> -αAl <sub>2</sub> O <sub>3</sub>	T = 500–700 °C P = 3-bar S/C = 1–4 Residence time = 1–8 kg <sub>cat</sub> ·s/mol	surface area = 4.5 m <sup>2</sup> /g <sub>cat</sub> bulk density = 680 kg/m <sup>3</sup> average porosity = 41%	@ S/C = 1, flow rate = 15 g/s, p = 3-bar, T = 700 °C						[72]
Raschig ring				X <sub>CH<sub>4</sub></sub> = 62%						
7-hole cylinder				X <sub>CH<sub>4</sub></sub> = 70%						
7-hole sphere				X <sub>CH<sub>4</sub></sub> = 75%						
1-hole cylinder	Ni = 20 wt %, CaO-Al <sub>2</sub> O <sub>3</sub> = 80 wt %	T = 500–850 °C P = 0.2–1 MPa S/C = 2–3.3 GHSV = 2–40 l CH <sub>4</sub> /(h·g <sub>cat</sub> )	surface area = 21.26 m <sup>2</sup> /g <sub>cat</sub> density = 1.8 g/cm <sup>3</sup> pore size = 111 Å	Equilibrium CH <sub>4</sub> conversion reached @ GHSV = 2 l CH <sub>4</sub> /(h·g <sub>cat</sub> ), T > 800 °C, P = 1 MPa, S/C = 3						[73]
cylinder-shaped alumina pellets	E-5Ni **	T = 700–800 °C S/C = 3 WHSV = 3000 mL/(g <sub>cat</sub> h)	Ni = 5.6 wt % Surface area = 204 m <sup>2</sup> /g	X <sub>CH<sub>4</sub></sub> = 96% @ 700 °C X <sub>CH<sub>4</sub></sub> = 99% @ 800 °C						[74]
	E-3.5Ni **			X <sub>CH<sub>4</sub></sub> = 96% @ 700 °C X <sub>CH<sub>4</sub></sub> = 97% @ 800 °C						
	E-3.5Ni-5Mg **			X <sub>CH<sub>4</sub></sub> = 95% @ 700 °C X <sub>CH<sub>4</sub></sub> = 98% @ 800 °C						
Micro-channel reactor Metal- ceramic plate	Ni = 15.87 wt %	T = 800–900 °C S/C = 3–5 P = 0.5–2 MPa GHSV = 40,000 to 240,000 h <sup>-1</sup>	Surface area = 108.75 m <sup>2</sup> /g Catalyst layer thickness = 70 mm	Equilibrium CH <sub>4</sub> conversion value and H <sub>2</sub> productivity = 0.1 m <sup>3</sup> /h @ T = 900 °C, GHSV = 240,000 h <sup>-1</sup> , P = 2 MPa, S/C = 3						[77]

\* T<sub>s</sub> = volume averaged temperature; Q<sub>sink</sub> = normalized heat sink; X<sub>CH<sub>4</sub></sub> = normalized CH<sub>4</sub> conversion; η<sub>i</sub> = effectiveness factors. \*\* Egg-Shell type Ni Distribution.

### 3.2.2. Ceramic Carriers

The research group of the University of Salerno very deeply investigated the possibility to intensify the MSR by using Ni based catalysts supported on silicon carbide (SiC) and cordierite monoliths. The authors, by setting-up an advanced experimental reaction system, preliminarily studied the influence of the geometric configuration of the monoliths, as well as the Ni loading and the washcoat presence [94]. The experimental tests showed that the monolith with “wall flow” (WF, the parallel channels are alternatively plugged at each end in order to force the reaction stream to flow through the inner porous walls) configuration had better performance in terms of hydrogen yields at the same temperature and GHSV with respect to the “flow through” (FT, the channels are open on both sides) configuration. In particular, the results highlighted that the preliminary deposition of a ceria-based washcoat on the support increases the specific surface area, thus allowing a better dispersion of the active species and consequently better catalytic activity, particularly at lower temperatures. Numerical models, which were developed and implemented by the software COMSOL Multiphysics, were used to compare these two geometries, and the results were in a quite good agreement with the kinetic analysis and experimental results, thus confirming the better performances of the WF configuration with respect to the FT [94]. These preliminary results demonstrated that the use of high thermal conductivity monolithic catalyst in wall flow configuration allowed to overcome the energy and mass limitations, which are the main bottlenecks of the commercial steam reforming catalysts. The Ni/CeO<sub>2</sub> wash-coated SiC monolithic catalysts (with only 5 wt % of Ni) also showed better performance in comparison with a commercial catalyst for MSR [95]. The catalytic activity tests showed that the use of structured catalysts, due to the well-known better heat transfer from the outside towards the inside, allowed for flattening of the radial thermal profile, since a reduced difference between oven and gas temperatures could be observed. This effect leads to a higher performance of the process that, under equal operating conditions, leads to higher methane conversion and hydrogen yield. The silicon carbide carriers in the “wall-flow” configuration showed higher catalytic activity than the other monoliths and the commercial catalyst, especially at temperatures below 750 °C. The use of Ceria/Alumina slurry for the wash-coating of the SiC monoliths, allowed for a further intensification in the MSR [96,97]. In fact, the 5 wt % Ni loaded SiC monoliths in wall flow configuration showed further better performance in terms of methane conversion and hydrogen yield in the temperature range 500–750 °C. These researches confirmed that the use of high thermal conductivity supports for Ni based structured catalysts may result in a feasible process intensification of the MSR, since the choice of these supports has the conjugated advantages of increasing the hydrogen yield and requires a lower temperature outside the reactor, allowing for an overall increase in the efficiency of the process. In this way, the optimization in catalytic volume management might lead to substantial performances increasing, which, in turn, assures a reduction in hydrogen production costs. The observed enhancements in thermal management inside the catalytic volume could result in practical application, not only in the steam reforming field: the minimization of heat transfer resistance could be achieved in all endothermic reactions, flattening the thermal profiles from the peripheral to the center of the catalytic bed, hence resulting in an improving of reaction control. Moreover, the ability of SiC monolith to redistribute temperature in the catalytic volume might reduce the risks that are linked to hotspot phenomena for oxidative reactions, (such as partial oxidation of hydrocarbons): the optimal reaction control results in an enhanced safety of the process, as well as in an improved catalyst lifetime.

Moon et al. also investigated the SiC as support for Ni based structured catalysts for MSR [98]. The authors prepared and tested in MSR 10 wt % Ni based catalysts, supported on calcium aluminate (CAx), which differ from each other by the carrier (with and without SiC). The results evidenced that the contemporary presence of CAx and SiC, as carrier, increased the thermal conductivity of the whole structured catalyst, thus allowing a higher catalytic activity in terms of methane conversion (>90%) and H<sub>2</sub> yield (>95%) as well as a higher coke resistance (coke formation <0.6%) at 750 °C, with respect to the other catalysts. These results confirmed that the Ni based catalysts supported on SiC could be promising candidates for producing hydrogen by the steam reforming of methane.

Other research groups also investigated the feasibility of ceramic supports different from SiC for the intensification of MSR. Ashraf et al. used ceramic monoliths ( $\alpha$ -alumina) with square channels (100 cpsi) and hexagonal channels (170 cpsi), diameter 9 mm, and length 30 mm, loaded with 100/150/200/250 mg of catalyst (Ru(1.5 wt %)/La(3 wt %)-Al<sub>2</sub>O<sub>3</sub>) [99]. The results evidenced that the better performance in terms of methane conversion, in all of the tested conditions (temperature range 600–900 °C, WHSV = 27–368 NL h<sup>-1</sup>gcat, molar steam to carbon ratio S/C = 3.0) was obtained with the catalyst loading of 100 mg (washcoat thickness of 58.5  $\mu$ m) and 150 mg (washcoat thickness of 78.9  $\mu$ m). These catalysts reached high methane conversion, approaching the thermodynamic equilibrium, at temperatures that were higher than 800 °C. The authors highlighted that the intensification of MSR could be obtained by using monoliths with high cell densities, since they can simultaneously increase the geometric surface area and the voidage, hence allowing a reduction of the thickness of the catalytic layer, in order to avoid internal mass transfer limitations.

Narataruksa et al. performed an interesting study to achieve optimal dimensions of a monolithic catalytic ceramic reactor for the highest rate of reaction in MSR [100]. The authors, by means of an analytical and CFD model, individuated the optimal length of a square channel monolithic reactor. The results of the analytical model showed that the optimal length was of 41.6 mm with a reaction rate of  $2.88 \times 10^{-8}$  mol/s at the channel height of 1.5 mm, 600 °C, and 1 atm; the results of the CFD model and the experimental tests evidenced an optimal channel length of 80.0 mm and 90.0 mm, respectively, with respective reaction rates of  $7.42 \times 10^{-7}$  mol/s and  $6.85 \times 10^{-7}$  mol/s. The CFD model was also used to investigate the effects of channel heights that ranged from 0.5 to 3.0 mm, by the definition of methane conversion per unit channel perimeter: the highest value (50% mm<sup>-1</sup>) is afforded at a channel height of 0.50 mm. The results of the CFD model can be summarized in the sense that a constant reaction rate was established at an L/H ratio of 53, while the experimental results that were performed with monoliths with different channels allowed for concluding that a constant reaction rate occurred at an L/H ratio of 60.

Nam et al. numerically investigated the effects of the washcoat properties, including the layer thickness (20–80  $\mu$ m), the mean pore diameter (10–40 nm), and the volume-specific catalyst surface area ( $1.1\text{--}3.3 \times 10^7$  m<sup>2</sup>/m<sup>3</sup>), in the Ni/MgAl<sub>2</sub>O<sub>4</sub> washcoat catalyst layers that were used in MSR conditions relevant to small-scale hydrogen production systems (1–3-bar pressure, 600–800 °C temperature, and 2–4 steam-to-carbon ratio) [101]. The authors used the intrinsic reaction kinetics (Xu and Froment model) and multicomponent mass diffusion (Maxwell-Stefan equation) in their simulations, and proposed correlation equations for easy evaluation of the effectiveness factors (presented as a function of the methane conversion ratio and effective Thiele moduli) coming from the simulations. The authors demonstrated that the proposed correlation equations could adequately estimate the effectiveness factor data that were obtained by numerical calculation, hence providing useful data for designing small-scale SMR systems and performing numerical simulations.

Leonzio developed an ANOVA analysis, in which an integrated Pd-based membrane reactor is considered for the MSR. The catalyst is a Ni(10)/CeLaZr catalyst that is supported on SSiC ceramic foam, and the reactor was modelled in MATLAB software while using the Numaguchi kinetic [102]. The results showed that only inlet temperature, methane flow rate, their interaction, and the thickness of membrane are significant in order to improve the performance of the reactor in terms of hydrogen yield, carbon dioxide conversion and methane conversion. In particular, methane conversion of 99%, carbon dioxide conversion of 40%, and hydrogen yield of 3.2 can be achieved with an inlet temperature equal to 823 °C, methane flow rate equal to 0.1 kmol/h, hydrogen permeability equal to  $3600 \text{ m}^3 \mu\text{m}^2 \text{ hr bar}^{0.5}$ , being chosen in order to have better performances of membrane, and a thickness equal to 0.003 m to reduce the costs.

Table 4 summarizes the main performances of the catalysts supported on ceramic carriers.

**Table 4.** Summary of the main performance of the catalysts supported on ceramic carries.

Structured Carrier Shape	Catalyst	Operating Conditions	Main Characteristics	Main Performance	Ref.
honeycomb	Ni/Ce	T = 450–650 °C S/C = 2 P = 1 atm	Surface area = 152 m <sup>2</sup> /g	X <sub>CH<sub>4</sub></sub> = 79.1% S <sub>CO</sub> = 59.4% S <sub>CO<sub>2</sub></sub> = 40.6% @ 650 °C	[75]
Rolled foils	Ni <sub>3</sub> Al	T = 600–800 °C S/C = 1 GHSV = 0.091 m <sup>3</sup> /(hm <sup>2</sup> )	total geometrical surface = 0.0066 m <sup>2</sup>	X <sub>CH<sub>4</sub></sub> = 90% S <sub>CO</sub> = 99% S <sub>CO<sub>2</sub></sub> = 2% @ 650 °C	[82]
Rolled foils	Ni	GHSV = 455–2880 h <sup>-1</sup> S/C = 0.62–2.48 T = 700–800 °C	Geometric surface area = 66.4 cm <sup>2</sup> Pore density = 700 cpsi specific surface area = 88.1 cm <sup>2</sup> /cm <sup>3</sup>	X <sub>CH<sub>4</sub></sub> = 94.0% S <sub>CO</sub> = 91.1% S <sub>CO<sub>2</sub></sub> = 8.9% H <sub>2</sub> yield = 77.6% H <sub>2</sub> production rate = 8.7 mL/min. H <sub>2</sub> production rate/Volume = 11.6 mL/min./cm <sup>3</sup> @ T = 800 °C, GHSV = 535 h <sup>-1</sup> , S/C = 1.24	[85]
Rolled foils	Ni	GHSV = 6400 h <sup>-1</sup> S/C = 1.362 T = 600–900 °C	Geometric surface area = 43.72 cm <sup>2</sup> Pore density = 2300 cpsi specific surface area = 87.2 cm <sup>2</sup> /cm <sup>3</sup>	X <sub>CH<sub>4</sub></sub> = 55.7% @ T = 800 °C	[86]
Rolled foils	Ni	GHSV = 6400 h <sup>-1</sup> S/C = 1.362 T = 600–900 °C	Geometric surface area = 43.72 cm <sup>2</sup> Pore density = 2300 cpsi specific surface area = 87.2 cm <sup>2</sup> /cm <sup>3</sup>	X <sub>CH<sub>4</sub></sub> = 90% @ T = 900 °C, Ni honeycomb catalysts steam treated at 900 °C for 1 h followed by H <sub>2</sub> reduction at 900 °C for 1 h	[87]

Table 4. Cont.

Structured Carrier Shape	Catalyst	Operating Conditions	Main Characteristics	Main Performance	Ref.
foam	Ni	$w_{\text{CH}_4}^0 = 21.28$ $w_{\text{H}_2\text{O}}^0 = 71.45$ $w_{\text{H}_2}^0 = 2.60$ $w_{\text{CO}}^0 = 1.19$ $w_{\text{N}_2}^0 = 3.48$ $T_0 = 550\text{ }^\circ\text{C}$ $P = 1\text{-bar}$	$\text{ppi} = 10$ $K_p = 1.2\text{ m}^2\text{ ***}$ $C_f = 0.097\text{ ***}$ $\rho_s = 8900\text{ Kg/m}^3\text{ ***}$ $\lambda_s = 71\text{ W/m K ***}$	$X_{\text{CH}_4} = 29.491\%$ $\text{H}_2\text{ production rate} = 47.645$	
	Ni-Cr	$w_{\text{CH}_4}^0 = 21.28$ $w_{\text{H}_2\text{O}}^0 = 71.45$ $w_{\text{H}_2}^0 = 2.60$ $w_{\text{CO}}^0 = 1.19$ $w_{\text{N}_2}^0 = 3.48$ $T_0 = 550\text{ }^\circ\text{C}$ $P = 1\text{-bar}$	$\text{ppi} = 20$ $K_p = 1.185\text{ m}^2\text{ ***}$ $C_f = 0.1\text{ ***}$ $\rho_s = 8420\text{ Kg/m}^3\text{ ***}$ $\lambda_s = 22.5\text{ W/m K ***}$	$X_{\text{CH}_4} = 22.534\%$ $\text{H}_2\text{ production rate} = 41.015$	[88]
	Ni-Fe-Cr	$w_{\text{CH}_4}^0 = 21.28$ $w_{\text{H}_2\text{O}}^0 = 71.45$ $w_{\text{H}_2}^0 = 2.60$ $w_{\text{CO}}^0 = 1.19$ $w_{\text{N}_2}^0 = 3.48$ $T_0 = 550\text{ }^\circ\text{C}$ $P = 1\text{-bar}$	$\text{ppi} = 10$ $K_p = 1.49\text{ m}^2\text{ ***}$ $C_f = 0.099\text{ ***}$ $\rho_s = 6285\text{ Kg/m}^3\text{ ***}$ $\lambda_s = 134.87\text{ W/m K ***}$	$X_{\text{CH}_4} = 37.400\%$ $\text{H}_2\text{ production rate} = 53.577$	
Fecralloy <sup>®</sup> monoliths	1.5 wt %Ru/3 wt %La-Al <sub>2</sub> O <sub>3</sub>	$T = 600\text{--}900\text{ }^\circ\text{C}$ $\text{WHSV} = 55\text{ NI}/(\text{h g}_{\text{cat}})$ $S/C = 3$	$\text{cpsi} = 461$ $\text{catalysts loading} = 109\text{ mg}$	$\text{Equilibrium CH}_4\text{ conversion values @ } 800\text{ }^\circ\text{C}$ $X_{\text{CH}_4} = 52\%$ $\text{@ } 600\text{ }^\circ\text{C}$	
		$T = 600\text{--}900\text{ }^\circ\text{C}$ $\text{WHSV} = 55\text{ NI}/(\text{h g}_{\text{cat}})$ $S/C = 3$	$\text{cpsi} = 461$ $\text{catalyst loading} = 171.8\text{ mg}$	$\text{Equilibrium CH}_4\text{ conversion values @ } 800\text{ }^\circ\text{C}$ $X_{\text{CH}_4} = 61\%$ $\text{@ } 600\text{ }^\circ\text{C}$	[89]
		$T = 600\text{--}900\text{ }^\circ\text{C}$ $\text{WHSV} = 55\text{ NI}/(\text{h g}_{\text{cat}})$ $S/C = 3$	$\text{cpsi} = 461$ $\text{catalyst loading} = 216.9\text{ mg}$	$\text{Equilibrium CH}_4\text{ conversion values @ } 800\text{ }^\circ\text{C}$ $X_{\text{CH}_4} = 62\%$ $\text{@ } 600\text{ }^\circ\text{C}$	

Table 4. Cont.

Structured Carrier Shape	Catalyst	Operating Conditions	Main Characteristics	Main Performance	Ref.
Membrane reformer with Ni foam	10 %Ni/10 %MgO/Ni-foam	P = 1-bar T = 400–600 °C S/C = 2	4 mm thick foam discs, 60 ppi	Equilibrium CH <sub>4</sub> conversion values @ 600 °C for the catalytic discs	[90]
FeCrAlloy monolith	0.5 wt %Rh-15 wt %Ni/MgAl <sub>2</sub> O <sub>4</sub>	T <sub>wall</sub> = 600 °C, P = 1-bar, S/C=5, GHSV = 6000 h <sup>-1</sup> and W/F <sub>ao</sub> = 0.34 g <sub>cat</sub> -h/gmol		X <sub>CH<sub>4</sub></sub> = 50% H <sub>2</sub> /CO = 37 H <sub>2</sub> /CO <sub>2</sub> = 4.6 S <sub>CO</sub> = 11.0 × 10 <sup>-2</sup>	[92]
Catalytic alumina egg-shell particles with diameter of 600 μm, filling the voids of FeCrAlY open cell foams of 12 PPI and copper open cell foams of 10 and 40 PPI	Rh/Al <sub>2</sub> O <sub>3</sub>	GHSV = 5000 and 10,000 h <sup>-1</sup> T = 600–800 °C S/C = 3.5	λ <sub>s</sub> = 16 W/(m K) – FeCrAlY foam λ <sub>s</sub> = 380 W/(m K) – Cu foam	WT* – CT* = 40 for Cu foam WT* – CT* = 50 for FeCrAlY foam X <sub>CH<sub>4</sub></sub> = 86.4% for Cu foam, X <sub>CH<sub>4</sub></sub> = 75% for FeCrAlY foam @ T <sub>oven</sub> = 700 °C	[93]
SiC monolith	30 wt %Ni	GHSV = 5000 to 25,000 h <sup>-1</sup> T = 600–800 °C P = 1-bar S/C = 3	Direct impregnation λ <sub>s</sub> = 350 W/(m K) – SiC monolith Flow through configuration	Equilibrium CH <sub>4</sub> conversion values for T > 800 °C	[94]
	20 wt %Ni/20 wt %CeO <sub>2</sub>	GHSV = 1250 to 5000 h <sup>-1</sup> T = 550–800 °C P = 1-bar S/C = 3	Washcoating + Ni direct impregnation λ <sub>s</sub> = 350 W/(m K) – SiC monolith Flow through and Wall Flow configuration	Equilibrium CH <sub>4</sub> conversion values for T > 800 °C - Flow Through Equilibrium CH <sub>4</sub> conversion values for T > 750 °C – wall Flow	
SiC monolith	5 wt %Ni/20 wt %CeO <sub>2</sub>	GHSV = 100,000 h <sup>-1</sup> T <sub>oven</sub> = 500–950 °C P = 1-bar S/C = 3	λ <sub>s</sub> = 350 W/(m K) Flow through and Wall Flow configuration	Equilibrium CH <sub>4</sub> conversion values at T <sub>gas</sub> = 800 °C (T <sub>oven</sub> = 900 °C) for both configurations	[95]

Table 4. Cont.

Structured Carrier Shape	Catalyst	Operating Conditions	Main Characteristics	Main Performance	Ref.
Cordierite monolith	5 wt %Ni/20 wt %CeO <sub>2</sub>	GHSV = 100,000 h <sup>-1</sup> T <sub>oven</sub> = 500–950 °C P = 1-bar S/C = 3	λ <sub>s</sub> = 3 W/(m K) Flow through configuration	X <sub>CH<sub>4</sub></sub> = 80% at T <sub>oven</sub> = 900 °C	
SiC monolith	5 wt %Ni/20 wt %CeO <sub>2</sub> /Al <sub>2</sub> O <sub>3</sub>	GHSV = 100,000 h <sup>-1</sup> T <sub>oven</sub> = 500–950 °C P = 1-bar S/C = 3	λ <sub>s</sub> = 350 W/(m K) Flow through and Wall Flow configuration	Equilibrium CH <sub>4</sub> conversion values at T <sub>gas</sub> = 750 °C (T <sub>oven</sub> = 850 °C) for the wall flow configuration	[96,97]
calcium aluminate modified SiC	10%Ni	GHSV = 30,000 h <sup>-1</sup> T = 650–850 °C P = 1-bar S/C = 1 to 3	1 mm granules λ <sub>s</sub> = 1.16 W/(m K)	X <sub>CH<sub>4</sub></sub> = 97.9 % at T = 650 °C and S/C = 3 X <sub>CH<sub>4</sub></sub> = 81.3 % at T = 850 °C and S/C = 1	[98]
αAlumina monolith	1.5 wt %Ru/ 3 wt %La-Al <sub>2</sub> O <sub>3</sub>	T = 600–900 °C S/C = 3 WHSV = 27 to 368 NI h <sup>-1</sup> g <sub>cat</sub> <sup>-1</sup>	Catalyst loading = 100 to 250 mg	Equilibrium CH <sub>4</sub> conversion values at T > 800 °C for 100 and 150 mg catalyst loadings	[99]

\* WT = wall thermocouple, CT = central thermocouple; \*\*\* K<sub>p</sub> = permeability, Cf = inertial loss coefficient, λ<sub>s</sub> = thermal conductivity

#### 4. Conclusions

The high activity and the low cost made Ni catalysts have been widely studied by the scientific community in MSR. Advancements in catalysis technologies and methods have improved the state of MSR, in particular the synthesis methods of nano-sized particles, including impregnation, co-sputtering, and chemical vapor deposition, allow for highly dispersed dopants and high activity. The researchers showed that the addition of metallic or bimetallic species to a Ni based catalyst can improve selectivity, durability, and activity, thus limiting the typical problems of the MSR, including coke formation, active oxidation, sintering, and segregation. This review evidenced that most common materials used as supports or support dopants are  $\text{CeO}_2$ ,  $\text{ZrO}_2$ , and their mixed oxides, since their high oxygen storage capacity and redox properties lead to efficient coke resistance, which makes these materials advantageous over conventionally used  $\text{Al}_2\text{O}_3$  or  $\text{MgAl}_2\text{O}_4$ .

The complexity of the traditional steam reforming process involving many very different operation units is optimized for the industrial scale, limiting the possibility to realize process intensification. In the last years, the scientific research focused on the development of innovative hydrogen production systems as well as on the optimization of the conventional processes and, in this sense, the catalyst has a fundamental role. In general, steam reforming catalysts must meet stringent requirements, such as high activity, reasonable life, good heat transfer, low pressure drop, high thermal stability, and excellent mechanical strength. In addition, the necessity of reducing the costs made the development of methane steam reforming processes operating at low temperature mandatory, so avoiding, for example, the use of special steel alloy. The development of new catalysts with well-defined properties is fundamental in order to reach this objective: in fact, the catalyst must activate methane at low temperature, it must drive its conversion up to equilibrium values at short contact times and, in addition, it must be resistant to deactivation factors (including carbon formation, which is favored at low temperature, and preferential oxidation, which occurs at low temperature mainly for Ni catalysts). The objective of a low temperature methane steam reforming can be reached by contemporarily separating a product, such as  $\text{H}_2$ , by means of membrane reactors, or  $\text{CO}_2$ , as in the case of sorption enhanced steam reforming process, since methane steam reforming at low reaction temperature results in low  $\text{CH}_4$  conversions due to thermodynamic limitations [1].

In the way of a process intensification, the main critical issue in a reforming plant must be overcome: in the MSR reforming process, the limiting step is the heat transfer towards the reaction volume, since its high endothermicity requires high heat fluxes, and the catalyst has low thermal conductivity. The final result is a thermal profile from the external to the middle of the catalytic bed. Such a constraint imposes complex reactor geometries and very high temperatures of heating medium, thus resulting in very expensive construction materials, very high reaction volumes, and very slow thermal transients. Therefore, it causes an increase of operative and fixed costs and a reduction of the overall process efficiency. The increasing interest in the development of compact methane steam reforming reactors for a distributed hydrogen economy calls for novel catalytic reactors with intensified heat management, which is, as said, the limiting factor of current process technology.

The use of high thermal conductivity carriers (such as monoliths or foams) is reported as a valuable general strategy for enhancing the performance of MSR. These carriers, in fact, assure a flatter axial thermal profile through the catalytic bed, leading to heat redistribution along it. In addition, the highly conductive supports ensure a more uniform radial temperature profile, thus resulting in better heat transfer and a reduction of hot-spot phenomena and very stable performance. The main studied carriers can be divided in two groups: (i) metallic and (ii) ceramic, with the latter ones being prevalently constituted by silicon carbide (SiC). All of the studies evidenced that the Ni-based catalytic metallic or SiC carriers can allow for obtaining higher methane conversion at a lower temperature with respect to the conventional packed bed catalysts, thus confirming the feasibility to use these innovative structured reactors for the valorization of small-scale methane sources as well as for distributed hydrogen production.

**Author Contributions:** Conceptualization, E.M. and M.M.; Ni based powder catalysts: M.M.; Ni based structured catalysts: E.M.; writing—original draft preparation, E.M.; writing—review and editing, E.M.; supervision, V.P. All authors have read and agree to the published version of the manuscript.

**Funding:** This research received no external funding.

**Conflicts of Interest:** The authors declare no conflict of interest.

## References

1. Angeli, S.D.; Monteleone, G.; Giaconia, A.; Lemonidou, A.A. State-of-the-art catalysts for CH<sub>4</sub> steam reforming at low temperature—Review. *Int. J. Hydrogen Energy* **2014**, *39*, 1979–1997. [[CrossRef](#)]
2. Sikander, U.; Sufian, S.; Salam, M.A. A review of hydrotalcite based catalysts for hydrogen production systems. *Int. J. Hydrogen Energy* **2017**, *42*, 19851–19868. [[CrossRef](#)]
3. Ma, Y.; Ma, Y.; Long, G.; Li, J.; Hu, X.; Ye, Z.; Wang, Z.; Buckley, C.E.; Dong, D. Synergistic promotion effect of MgO and CeO<sub>2</sub> on nanofibrous Ni/Al<sub>2</sub>O<sub>3</sub> catalysts for methane partial oxidation. *Fuel* **2019**, *258*, 116103. [[CrossRef](#)]
4. Palma, V.; Miccio, M.; Ricca, A.; Meloni, E.; Ciambelli, P. Monolithic catalysts for methane steam reforming intensification: Experimental and numerical investigations. *Fuel* **2014**, *138*, 80–90. [[CrossRef](#)]
5. Alvarez-Galvan, C.; Melian, M.; Ruiz-Matas, L.; Eslava, J.L.; Navarro, R.M.; Ahmadi, M.; Roldan Cuenya, B.; Fierro, J.L.G. Partial Oxidation of Methane to Syngas Over Nickel-Based Catalysts: Influence of Support Type, Addition of Rhodium, and Preparation Method. *Front. Chem.* **2019**, *7*, 1–16. [[CrossRef](#)]
6. Pinheiro, A.L.; Pinheiro, A.N.; Valentini, A.; Filho, J.M.; de Sousa, F.F.; de Sousa, J.R.; Rocha, M.; da Graça, C.; Bargiela, P.; Oliveira, A.C. Analysis of coke deposition and study of the structural features of MAI<sub>2</sub>O<sub>4</sub> catalysts for the dry reforming of methane. *Catal. Commun.* **2009**, *11*, 11–14. [[CrossRef](#)]
7. Hu, D.; Liu, C.; Li, L.; Lv, K.-L.; Zhang, Y.-H.; Li, J.-L. Carbon dioxide reforming of methane over nickel catalysts supported on TiO<sub>2</sub>(001) nanosheets. *Int. J. Hydrogen Energy* **2018**, *43*, 21345–21354. [[CrossRef](#)]
8. Lercher, J.A.; Bitter, J.H.; Hally, W.; Niessen, W.; Seshan, K. Design of stable catalysts for methane-carbon dioxide reforming. *Stud. Surf. Sci. Catal.* **1996**, *101*, 463–472. [[CrossRef](#)]
9. Pinheiro, A.N.; Valentini, A.; Sasaki, J.M.; Oliveira, A.C. Highly stable dealuminated zeolite support for the production of hydrogen by dry reforming of methane. *Appl. Catal. A Gen.* **2009**, *355*, 156–168. [[CrossRef](#)]
10. Ramezani, Y.; Meshkani, F.; Rezaei, M. Promotional effect of Mg in trimetallic nickelmanganese-magnesium nanocrystalline catalysts in CO<sub>2</sub> reforming of methane. *Int. J. Hydrogen Energy* **2018**, *43*, 22347–22356. [[CrossRef](#)]
11. Alrafe, B.; Polaert, I.; Ledoux, A.; Azzolina-Jury, F. Remarkably stable and efficient Ni and Ni-Co catalysts for CO<sub>2</sub> methanation. *Catal. Today* **2019**. [[CrossRef](#)]
12. Oton, L.F.; Coelho, D.C.; Oliveira Alcinea, C.; de Araujo, J.C.S.; Lang, R.; Rodríguez-Castellón, E.; Rodríguez-Aguado, E.; Lucrecio, A.F.; Assaf, E.M.; Reyna-Alvarado, J.; et al. Structural transformation of vanadate nanotubes into vanadate oxides nanostructures during the dry reforming of methane. *Mol. Catal.* **2020**, *480*, 110641. [[CrossRef](#)]
13. Rezaei, R.; Moradi, G. Study of the performance of dry methane reforming in a microchannel reactor using sputtered Ni/Al<sub>2</sub>O<sub>3</sub> coating on stainless steel. *Int. J. Hydrogen Energy* **2018**, *43*, 21374–21385. [[CrossRef](#)]
14. Chotirach, M.; Tungasmita, S.; Tungasmita, D.N.; Tantayanon, S. Titanium nitride promoted Ni-based SBA-15 catalyst for dry reforming of methane. *Int. J. Hydrogen Energy* **2018**, *43*, 21322–21332. [[CrossRef](#)]
15. Sepehri, S.; Rezaei, M.; Wang, Y.; Younesi, A.; Arandiyan, H. The evaluation of autothermal methane reforming for hydrogen production over Ni/CeO<sub>2</sub> catalysts. *Int. J. Hydrogen Energy* **2018**, *43*, 22340–22346. [[CrossRef](#)]
16. Ali, S.; Al-Marri, M.J.; Abdelmoneim, A.J.; Kumar, A.; Khader, M.M. Catalytic evaluation of nickel nanoparticles in methane steam reforming. *Int. J. Hydrogen Energy* **2016**, *41*, 22876–22885. [[CrossRef](#)]
17. Katheria, S.; Gupta, A.; Deo, G.; Kunzru, D. Effect of calcination temperature on stability and activity of Ni/MgAl<sub>2</sub>O<sub>4</sub> catalyst for steam reforming of methane at high pressure condition. *Int. J. Hydrogen Energy* **2016**, *41*, 14123–14132. [[CrossRef](#)]
18. Rogers, J.L.; Mangarella, M.C.; D'Amico, A.D.; Gallagher, J.R.; Dutzer, M.R.; Stavitski, E.; Miller, J.T.; Sievers, C. Differences in the Nature of Active Sites for Methane Dry Reforming and Methane Steam Reforming over Nickel Aluminate Catalysts. *ACS Catal.* **2016**, *6*, 5873–5886. [[CrossRef](#)]

19. Pechini, M.P. Method of Preparing Lead and Alkaline Earth Titanates and Niobates and Coating Method Using the Same to Form a Capacitor. U.S. Patent 3,3306,97A, 11 July 1967.
20. Khani, Y.; Shariatnia, Z.; Bahadoran, F. High catalytic activity and stability of ZnLaAlO<sub>4</sub> supported Ni, Pt and Ru nanocatalysts applied in the dry, steam and combined dry-steam reforming of methane. *Chem. Eng. J.* **2016**, *299*, 353–366. [CrossRef]
21. Fang, X.; Zhang, X.; Guo, Y.; Chen, M.; Liu, W.; Xu, X.; Peng, H.; Gao, Z.; Wang, X.; Li, C. Highly active and stable Ni/Y<sub>2</sub>Zr<sub>2</sub>O<sub>7</sub> catalysts for methane steam reforming: On the nature and effective preparation method of the pyrochlore support. *Int. J. Hydrogen Energy* **2016**, *41*, 11141–11153. [CrossRef]
22. Thalinger, R.; Gocyla, M.; Heggen, M.; Dunin-Borkowski, R.; Grünbacher, M.; Stöger-Pollach, M.; Schmidmair, D.; Klötzer, B.; Penner, S. Ni–perovskite interaction and its structural and catalytic consequences in methane steam reforming and methanation reactions. *J. Catal.* **2016**, *337*, 26–35. [CrossRef]
23. Yoo, J.; Park, S.; Hwan Song, J.; Yoo, S.; Kyu Song, I. Hydrogen production by steam reforming of natural gas over butyric acid-assisted nickel/alumina catalyst. *Int. J. Hydrogen Energy* **2017**, *42*, 28377–28385. [CrossRef]
24. Iglesias, I.; Baronetti, G.; Marino, F. Ni/Ce<sub>0.95</sub>M<sub>0.05</sub>O<sub>2-d</sub> (M = Zr, Pr, La) for methane steam reforming at mild conditions. *Int. J. Hydrogen Energy* **2017**, *42*, 29735–29744. [CrossRef]
25. Aghayan, M.; Potemkin, D.I.; Rubio-Marcos, F.; Uskov, S.I.; Snytnikov, P.V.; Hussainova, I. Template-Assisted Wet-Combustion Synthesis of Fibrous Nickel Based Catalyst for Carbon Dioxide Methanation and Methane Steam Reforming. *ACS Appl. Mater. Interfaces* **2017**, *9*, 43553–43562. [CrossRef]
26. Park, Y.S.; Kang, M.; Byeon, P.; Chung, S.Y.; Nakayama, T.; Ko, T.; Hwang, H. Fabrication of a regenerable Ni supported NiO-MgO catalyst for methane steam reforming by exsolution. *J. Power Sources* **2018**, *397*, 318–324. [CrossRef]
27. Zhang, X.; Peng, L.; Fang, X.; Cheng, Q.; Liu, W.; Peng, H.; Gao, Z.; Zhou, W.; Wang, X. Ni/Y<sub>2</sub>B<sub>2</sub>O<sub>7</sub> (B=Ti, Sn, Zr and Ce) catalysts for methane steam reforming: On the effects of B site replacement. *Int. J. Hydrogen Energy* **2018**, *43*, 8298–8312. [CrossRef]
28. Chen, C.; Wang, X.; Chen, X.; Liang, X.; Zou, X.; Lu, X. Combined steam and CO<sub>2</sub> reforming of methane over one-pot prepared Ni/La-Si catalysts. *Int. J. Hydrogen Energy* **2019**, *44*, 4780–4793. [CrossRef]
29. Fang, X.; Xu, L.; Zhang, X.; Zhang, K.; Dai, H.; Liu, W.; Xu, X.; Wang, X.; Zhou, W. Effect of rare earth element (Ln = La, Pr, Sm, and Y) on physicochemical properties of the Ni/Ln<sub>2</sub>Ti<sub>2</sub>O<sub>7</sub> catalysts for the steam reforming of methane. *Mol. Catal.* **2019**, *468*, 130–138. [CrossRef]
30. Iglesias, I.; Baronetti, G.; Alemany, L.; Mariño, F. Insight into Ni/Ce<sub>1-x</sub>Zr<sub>x</sub>O<sub>2-δ</sub> support interplay for enhanced methane steam reforming. *Int. J. Hydrogen Energy* **2019**, *44*, 3668–3680. [CrossRef]
31. Iglesias, I.; Forti, M.; Baronetti, G.; Mariño, F. Zr-enhanced stability of ceria based supports for methane steam reforming at severe reaction conditions. *Int. J. Hydrogen Energy* **2019**, *44*, 8121–8132. [CrossRef]
32. Sebai, I.; Boulahaouache, A.; Trari, M.; Salhi, N. Preparation and characterization of 5%Ni/γ-Al<sub>2</sub>O<sub>3</sub> catalysts by complexation with NH<sub>3</sub> derivatives active in methane steam reforming. *Int. J. Hydrogen Energy* **2019**, *44*, 9949–9958. [CrossRef]
33. Dan, M.; Mihet, M.; Lazar, M.D. Hydrogen and/or syngas production by combined steam and dry reforming of methane on nickel catalysts. *Int. J. Hydrogen Energy* **2020**. [CrossRef]
34. Hu, Y.H.; Ruckenstein, E. Catalytic Conversion of Methane to Synthesis Gas by Partial Oxidation and CO<sub>2</sub> Reforming. *Adv. Catal.* **2004**, *48*, 297–345. [CrossRef]
35. Rostrup-Nielsen, J.R. New aspects of syngas production and use. *Catal. Today* **2000**, *63*, 159–164. [CrossRef]
36. Liu, C.-J.; Ye, J.; Jiang, J.; Pan, Y. Progresses in the Preparation of Coke Resistant Ni-based Catalyst for Steam and CO<sub>2</sub> Reforming of Methane. *ChemCatChem* **2011**, *3*, 529–541. [CrossRef]
37. Lighthart, D.A.J.M.; Pieterse, J.A.Z.; Hensen, E.J.M. The role of promoters for Ni catalysts in low temperature (membrane) steam methane reforming. *Appl. Catal. A Gen.* **2011**, *405*, 108–119. [CrossRef]
38. Weststrate, C.J.; Saib, A.M.; Niemantsverdriet, J.W. Promoter segregation in Pt and Ru promoted cobalt model catalysts during oxidation–reduction treatments. *Catal. Today* **2013**, *215*, 2–7. [CrossRef]
39. Available online: <https://www.britannica.com/science/promoter-catalysis> (accessed on 14 March 2020).
40. Morales-Cano, F.; Lundegaard, L.F.; Tiruvalam, R.R.; Falsig, H.; Skjøth-Rasmussen, M.S. Improving the sintering resistance of Ni/Al<sub>2</sub>O<sub>3</sub> steam-reforming catalysts by promotion with noble metals. *Appl. Catal. A Gen.* **2015**, *498*, 117–125. [CrossRef]

41. Lertwittayanon, K.; Youravong, W.; Jye Lau, W. Enhanced catalytic performance of Ni/ $\alpha$ -Al<sub>2</sub>O<sub>3</sub> catalyst modified with CaZrO<sub>3</sub> nanoparticles in steam-methane reforming. *Int. J. Hydrogen Energy* **2017**, *42*, 28254–28265. [[CrossRef](#)]
42. Jaiswar, V.K.; Katheria, S.; Deo, G.; Kunzru, D. Effect of Pt doping on activity and stability of Ni/MgAl<sub>2</sub>O<sub>4</sub> catalyst for steam reforming of methane at ambient and high pressure condition. *Int. J. Hydrogen Energy* **2017**, *42*, 18968–18976. [[CrossRef](#)]
43. Azancot, L.; Bobadilla, L.F.; Santos, J.L.; Cordoba, J.M.; Centeno, M.A.; Odriozola, J.A. Influence of the preparation method in the metal-support interaction and reducibility of Ni-Mg-Al based catalysts for methane steam reforming. *Int. J. Hydrogen Energy* **2019**, *44*, 19827–19840. [[CrossRef](#)]
44. Boudjeloud, M.; Boulahouache, A.; Rabia, C.; Salhi, N. La-doped supported Ni catalysts for steam reforming of methane. *Int. J. Hydrogen Energy* **2019**, *44*, 9906–9913. [[CrossRef](#)]
45. Nazari, M.; Mehdi Alavi, S. An investigation of the simultaneous presence of Cu and Zn in different Ni/Al<sub>2</sub>O<sub>3</sub> catalyst loads using Taguchi design of experiment in steam reforming of methane. *Int. J. Hydrogen Energy* **2020**, *45*, 691–702. [[CrossRef](#)]
46. Phanawadee, P.; Laipraseard, K.; Yablonsky, G.S.; Constales, D.; Jamroonrote, W.; Jaipet, P. Estimation of the remaining lifetime of deactivated catalyst via the spatial average catalyst activity illustrated by the water–gas shift and steam methane reforming processes. *Reac. Kinet. Mech. Cat.* **2017**, *121*, 371–385. [[CrossRef](#)]
47. Argyle, M.D.; Bartholomew, C.H. Heterogeneous Catalyst Deactivation and Regeneration: A Review. *Catalysts* **2015**, *5*, 145–269. [[CrossRef](#)]
48. Ochoa, A.; Bilbao, J.; Gayubo, A.G.; Castano, P. Coke formation and deactivation during catalytic reforming of biomass and waste pyrolysis products: A review. *Renew. Sustain. Energy Rev.* **2020**, *119*, 109600. [[CrossRef](#)]
49. Hashemnejad, S.M.; Parvari, M. Deactivation and Regeneration of Nickel-Based Catalysts for Steam-Methane Reforming. *Chin. J. Catal.* **2011**, *32*, 273–279. [[CrossRef](#)]
50. Jablonski, W.S.; Villano, S.M.; Dean, A.M. A comparison of H<sub>2</sub>S, SO<sub>2</sub>, and COS poisoning on Ni/YSZ and Ni/K<sub>2</sub>O-CaAl<sub>2</sub>O<sub>4</sub> during methane steam and dry reforming. *Appl. Cat. A General* **2015**, *502*, 399–409. [[CrossRef](#)]
51. Yang, X. An experimental investigation on the deactivation and regeneration of a steam reforming catalyst. *Renew. Energy* **2017**, *112*, 17–24. [[CrossRef](#)]
52. Laprune, D.; Theodoridi, C.; Tuel, A.; Farrusseng, D.; Meunier, F.C. Effect of polyaromatic tars on the activity for methane steam reforming of nickel particles embedded in silicalite-1. *Appl. Catal. B Environ.* **2017**, *204*, 515–524. [[CrossRef](#)]
53. Li, S.; Burel, L.; Aquino, C.; Tuel, A.; Morfin, F.; Rousset, J.-L.; Farrusseng, D. Ultimate size control of encapsulated gold nanoparticles. *Chem. Commun.* **2013**, *49*, 8507–8509. [[CrossRef](#)] [[PubMed](#)]
54. Haynes, D.J.; Shekhawat, D.; Berry, D.; Roy, A.; Spivey, J.J. Effect of calcination temperature on steam reforming activity of Ni-based pyrochlore catalysts. *J. Rare Earths* **2019**. [[CrossRef](#)]
55. Hernandez, A.D.; Kaisalo, N.; Simell, P.; Scarsella, M. Effect of H<sub>2</sub>S and thiophene on the steam reforming activity of nickel and rhodium catalysts in a simulated coke oven gas stream. *Appl. Cat. B Environ.* **2019**, *258*, 117977. [[CrossRef](#)]
56. Turchetti, L.; Murmura, M.A.; Monteleone, G.; Giaconia, A.; Lemonidou, A.A.; Angeli, S.D.; Palma, V.; Ruocco, C.; Annesini, M.C. Kinetic assessment of Ni-based catalysts in low-temperature methane/biogas steam reforming. *Int. J. Hydrogen Energy* **2016**, *41*, 16865–16877. [[CrossRef](#)]
57. Kechagiopoulos, P.N.; Angeli, S.D.; Lemonidou, A.A. Low temperature steam reforming of methane: A combined isotopic and microkinetic study. *Appl. Cat. B Environ.* **2017**, *205*, 238–253. [[CrossRef](#)]
58. Mundhwa, M.; Thurgood, C.P. Methane steam reforming at low steam to carbon ratios over alumina and yttria-stabilized-zirconia supported nickel-spinel catalyst: Experimental study and optimization of microkinetic model. *Fuel Process. Technol.* **2017**, *168*, 27–39. [[CrossRef](#)]
59. German, E.D.; Sheintuch, M. Methane steam reforming rates over Pt, Rh and Ni(111) accounting for H tunneling and for metal lattice vibrations. *Surf. Sci.* **2017**, *656*, 126–139. [[CrossRef](#)]
60. Thallam Thattai, A.; van Biert, L.; Aravind, P.V. On direct internal methane steam reforming kinetics in operating solid oxide fuel cells with nickel-ceria anodes. *J. Power Sources* **2017**, *370*, 71–86. [[CrossRef](#)]

61. Che, F.; Gray, J.T.; Ha, S.; McEwen, J.-S. Reducing Reaction Temperature, Steam Requirements, and Coke Formation During Methane Steam Reforming Using Electric Fields: A Microkinetic Modeling and Experimental Study. *ACS Catal.* **2017**, *7*, 6957–6968. [[CrossRef](#)]
62. Khzouz, M.; Gkanas, E.I. Experimental and Numerical Study of Low Temperature Methane Steam Reforming for Hydrogen Production. *Catalysts* **2018**, *8*, 5. [[CrossRef](#)]
63. Ji, G.; Zhao, M.; Wang, G. Computational fluid dynamic simulation of a sorption-enhanced palladium membrane reactor for enhancing hydrogen production from methane steam reforming. *Energy* **2018**, *147*, 884–895. [[CrossRef](#)]
64. De Oliveira Rocha, K.; Marques, C.M.P.; Correa Bueno, J.M. Effect of Au doping of Ni/Al<sub>2</sub>O<sub>3</sub> catalysts used in steam reforming of methane: Mechanism, apparent activation energy, and compensation effect. *Chem. Eng. Sci.* **2019**, *207*, 844–852. [[CrossRef](#)]
65. Pashchenko, D. Combined methane reforming with a mixture of methane combustion products and steam over a Ni-based catalyst: An experimental and thermodynamic study. *Energy* **2019**, *185*, 573–584. [[CrossRef](#)]
66. Pashchenko, D. Numerical study of steam methane reforming over a pre-heated Ni-based catalyst with detailed fluid dynamics. *Fuel* **2019**, *236*, 686–694. [[CrossRef](#)]
67. Unruean, P.; Plianwong, T.; Pruksawan, S.; Kitiyanan, B.; Ziff, R.M. Kinetic Monte-Carlo Simulation of Methane Steam Reforming over a Nickel Surface. *Catalysts* **2019**, *9*, 946. [[CrossRef](#)]
68. Liu, L.; Hong, D.; Guo, X. Insight into CaO addition on coking resistance of Ni surface for sorption enhanced methane steam reforming: A density functional study. *Appl. Surf. Sci.* **2019**, *475*, 887–895. [[CrossRef](#)]
69. Vogt, C.; Kranenborg, J.; Monai, M.; Weckhuysen, B.M. Structure Sensitivity in Steam and Dry Methane Reforming over Nickel: Activity and Carbon Formation. *ACS Catal.* **2020**, *10*, 1428–1438. [[CrossRef](#)]
70. Chen, K.; Zhao, Y.; Zhang, W.; Feng, D.; Sun, S. The intrinsic kinetics of methane steam reforming over a nickel-based catalyst in a micro fluidized bed reaction system. *Int. J. Hydrogen Energy* **2020**, *45*, 1615–1628. [[CrossRef](#)]
71. Karthik, G.M.; Buwa, V. Particle-Resolved Simulations of Methane Steam Reforming in Multilayered Packed Beds. *AIChE J.* **2018**, *64*, 4162–4176. [[CrossRef](#)]
72. Pashchenko, D. Experimental investigation of reforming and flow characteristics of a steam methane reformer filled with nickel catalyst of various shapes. *Energy Convers. Manag.* **2019**, *185*, 465–472. [[CrossRef](#)]
73. Park, H.-G.; Han, S.-Y.; Jun, K.-W.; Woo, Y.; Park, M.-J.; Kim, S.K. Bench-Scale Steam Reforming of Methane for Hydrogen Production. *Catalysts* **2019**, *9*, 615. [[CrossRef](#)]
74. Kim, Y.; Cho, E.; Ko, C.H. Preparation of Ni-based egg-shell-type catalyst on cylinder-shaped alumina pellets and its application for hydrogen production via steam methane reforming. *Int. J. Hydrogen Energy* **2019**, *44*, 5314–5323. [[CrossRef](#)]
75. Fukuhara, C.; Yamamoto, K.; Makiyama, Y.; Kawasaki, W.; Watanabe, R. A metal-honeycomb-type structured catalyst for steam reforming of methane: Effect of preparation condition change on reforming performance. *Appl. Catal. A Gen.* **2015**, *492*, 190–200. [[CrossRef](#)]
76. Gouveia Gil, A.; Wu, Z.; Chadwick, D.; Li, K. Microstructured Catalytic Hollow Fiber Reactor for Methane Steam Reforming. *Ind. Eng. Chem. Res.* **2015**, *54*, 5563–5571. [[CrossRef](#)]
77. Zhang, N.; Chen, X.; Chu, B.; Cao, C.; Jin, Y.; Cheng, Y. Catalytic performance of Ni catalyst for steam methane reforming in a micro-channel reactor at high pressure. *Chem. Eng. Process. Process. Intensif.* **2017**, *118*, 19–25. [[CrossRef](#)]
78. Calisan, A.; Ogulgonen, C.G.; Yilmaz, A.; Uner, D.; Kincal, S. Steam methane reforming over structured reactors under concentrated solar irradiation. *Int. J. Hydrogen Energy* **2019**, *44*, 18682–18693. [[CrossRef](#)]
79. Wismann, S.T.; Engbæk, J.S.; Vendelbo, S.B.; Bendixen, F.B.; Eriksen, W.L.; Aasberg-Petersen, K.; Frandsen, C.; Chorkendor, I.; Mortensen, P.M. Electrified methane reforming: A compact approach to greener industrial hydrogen production. *Science* **2019**, *364*, 756–759. [[CrossRef](#)]
80. Kumar, A.; Baldea, M.; Edgar, T.F. A physics-based model for industrial steam-methane reformer optimization with non-uniform temperature field. *Comput. Chem. Eng.* **2017**, *105*, 224–236. [[CrossRef](#)]
81. Govender, S.; Friedrich, H.B. Monoliths: A Review of the Basics, Preparation Methods and Their Relevance to Oxidation (review). *Catalysts* **2017**, *7*, 62. [[CrossRef](#)]

82. Xu, Y.; Ma, Y.; Demura, M.; Hirano, T. Enhanced catalytic activity of Ni<sub>3</sub>Al foils towards methane steam reforming by water vapor and hydrogen pretreatments. *Int. J. Hydrogen Energy* **2016**, *41*, 7352–7362. [[CrossRef](#)]
83. Mundhwa, M.; Parmar, R.D.; Thurgood, C.P. A comparative parametric study of a catalytic plate methane reformer coated with segmented and continuous layers of combustion catalyst for hydrogen production. *J. Power Sources* **2017**, *344*, 85–102. [[CrossRef](#)]
84. Mundhwa, M.; Thurgood, C.P. Numerical study of methane steam reforming and methane combustion over the segmented and continuously coated layers of catalysts in a plate reactor. *Fuel Process. Technol.* **2017**, *158*, 57–72. [[CrossRef](#)]
85. Hirano, T.; Xu, Y. Catalytic properties of a pure Ni coil catalyst for methane steam reforming. *Int. J. Hydrogen Energy* **2017**, *42*, 30621–30629. [[CrossRef](#)]
86. Xu, Y.; Harimoto, T.; Hirano, T.; Ohata, H.; Kunieda, H.; Hara, Y.; Miyata, Y. Catalytic performance of a high-cell-density Ni honeycomb catalyst for methane steam reforming. *Int. J. Hydrogen Energy* **2018**, *43*, 15975–15984. [[CrossRef](#)]
87. Xu, Y.; Harimoto, T.; Wang, L.; Hirano, T.; Kunieda, H.; Hara, Y.; Miyata, Y. Effect of steam and hydrogen treatments on the catalytic activity of pure Ni honeycomb for methane steam reforming. *Chem. Eng. Process. Process. Intensif.* **2018**, *129*, 63–70. [[CrossRef](#)]
88. Settar, A.; Abboudi, S.; Lebaal, N. Effect of inert metal foam matrices on hydrogen production intensification of methane steam reforming process in wall-coated reformer. *Int. J. Hydrogen Energy* **2018**, *43*, 12386–12397. [[CrossRef](#)]
89. Ashraf, M.A.; Sanz, O.; Montes, M.; Specchia, S. Insights into the effect of catalyst loading on methane steam reforming and controlling regime for metallic catalytic monoliths. *Int. J. Hydrogen Energy* **2018**, *43*, 11778–11792. [[CrossRef](#)]
90. Shigarov, A.B.; Kirillov, V.A.; Amosov, Y.I.; Brayko, A.S.; Avakov, V.B.; Landgraf, I.K.; Urusov, A.R.; Jivulko, S.A.; Izmaylovich, V.V. Membrane reformer module with Ni-foam catalyst for pure hydrogen production from methane: Experimental demonstration and modelling. *Int. J. Hydrogen Energy* **2017**, *42*, 6713–6728. [[CrossRef](#)]
91. Pajak, M.; Mozdziejcz, M.; Chalusiak, M.; Kimijima, S.; Szmyd, J.S.; Brus, G. A numerical analysis of heat and mass transfer processes in a macro-patterned methane/steam reforming reactor. *Int. J. Hydrogen Energy* **2018**, *43*, 20474–20487. [[CrossRef](#)]
92. Katheria, S.; Deo, G.; Kunzru, D. Rh-Ni/MgAl<sub>2</sub>O<sub>4</sub> catalyst for steam reforming of methane: Effect of Rh doping, calcination temperature and its application on metal monoliths. *Appl. Catal. A* **2019**, *570*, 308–318. [[CrossRef](#)]
93. Balzarotti, R.; Ambrosetti, M.; Beretta, A.; Groppi, G.; Tronconi, E. Investigation of packed conductive foams as a novel reactor configuration for methane steam reforming. *Chem. Eng. J.* **2019**. [[CrossRef](#)]
94. Palma, V.; Ricca, A.; Meloni, E.; Martino, M.; Miccio, M.; Ciambelli, P. Experimental and numerical investigations on structured catalysts for methane steam reforming intensification. *J. Clean. Prod.* **2016**, *111*, 217–230. [[CrossRef](#)]
95. Ricca, A.; Palma, V.; Martino, M.; Meloni, E. Innovative catalyst design for methane steam reforming intensification. *Fuel* **2017**, *198*, 175–182. [[CrossRef](#)]
96. Palma, V.; Ricca, A.; Martino, M.; Meloni, E. Innovative structured catalytic systems for methane steam reforming intensification. *Chem. Eng. Process. Process. Intensif.* **2017**, *120*, 207–215. [[CrossRef](#)]
97. Palma, V.; Martino, M.; Meloni, E.; Ricca, A. Novel structured catalysts configuration for intensification of steam reforming of methane. *Int. J. Hydrogen Energy* **2017**, *42*, 1629–1638. [[CrossRef](#)]
98. Noh, Y.S.; Lee, K.-Y.; Moon, D.J. Hydrogen production by steam reforming of methane over nickel based structured catalysts supported on calcium aluminate modified SiC. *Int. J. Hydrogen Energy* **2019**, *44*, 21010–21019. [[CrossRef](#)]
99. Ashraf, M.A.; Sanz, O.; Italiano, C.; Vita, A.; Montes, M.; Specchia, S. Analysis of Ru/La-Al<sub>2</sub>O<sub>3</sub> catalyst loading on alumina monoliths and controlling regimes in methane steam reforming. *Chem. Eng. J.* **2018**, *334*, 1792–1807. [[CrossRef](#)]
100. Inbamrung, P.; Sornchamni, T.; Prapainainar, C.; Tungkamani, S.; Narataruksa, P.; Jovanovic, G.N. Modeling of a square channel monolith reactor for methane steam reforming. *Energy* **2018**, *152*, 383–400. [[CrossRef](#)]

101. Jeong, A.; Shin, D.; Baek, S.M.; Nam, J.H. Effectiveness factor correlations from simulations of washcoat nickel catalyst layers for small-scale steam methane reforming applications. *Int. J. Hydrogen Energy* **2018**, *43*, 15398–15411. [[CrossRef](#)]
102. Leonzio, G. ANOVA analysis of an integrated membrane reactor for hydrogen production by methane steam reforming. *Int. J. Hydrogen Energy* **2019**, *44*, 11535–11545. [[CrossRef](#)]



© 2020 by the authors. Licensee MDPI, Basel, Switzerland. This article is an open access article distributed under the terms and conditions of the Creative Commons Attribution (CC BY) license (<http://creativecommons.org/licenses/by/4.0/>).